



29 backtracking, and nucleosome hopping between wrapped states. While H2A.Z widens the barrier,  
30 uH2B heightens it, and both modifications greatly lengthen Pol II crossing time. Using the dwell  
31 times of Pol II at each nucleosomal position we extract the energetics of the barrier. The  
32 orthogonal barrier modifications of H2A.Z and uH2B, and their effects on Pol II dynamics  
33 rationalize their observed enrichment in +1 nucleosomes and suggest a mechanism for selective  
34 control of gene expression.

35

## 36 **Keywords**

37 High-resolution optical tweezers, single molecule unzipping, nucleosome barrier, Pol II  
38 transcription, histone variant H2A.Z, ubiquitinated H2B, ‘Molecular ruler’, nucleosome  
39 topography maps, transcription regulation

40

## 41 **Highlights**

- 42 1. A single-molecule unzipping assay mimics DNA unwinding by Pol II and maps the  
43 topography of human canonical, H2A.Z and uH2B nucleosome barriers at high resolution
- 44 2. Real-time dynamics and full molecular trajectories of Pol II crossing the nucleosomal barrier  
45 reveal the transcriptional landscape of the barrier at high accuracy
- 46 3. H2A.Z enhances the width and uH2B the height of the barrier
- 47 4. A unified mechanical model links position-dependent dwell times of Pol II on the  
48 nucleosome with energetics of the barrier

49

## 50 **Main**

51 The organization of genomic DNA into nucleosomes represents the main physical barrier to  
52 transcription by Pol II and constitutes a fundamental mechanism for regulation of gene  
53 expression in eukaryotes. In canonical (hereafter referred to as WT) nucleosomes, a core histone  
54 octamer made up of two copies of histones H2A, H2B, H3 and H4, is wrapped by ~147 basepairs  
55 (bp) of DNA. Variations in DNA sequence, wrapping strength asymmetry, and position-

56 dependent histone-DNA interactions are collectively responsible for the uneven character and  
57 polarity of the nucleosomal barrier to an elongating polymerase<sup>1-3</sup>. The topography of the  
58 nucleosomal barrier can be described using two parameters: its height at each position (i.e., the  
59 magnitude of the energy required to access the DNA) and its width (i.e., extension along the  
60 DNA). Although Pol II has been shown to be capable of transcribing through the nucleosome  
61 both *in vitro*<sup>1</sup> and *in vivo*<sup>4</sup>, the detailed, high-resolution dynamics of Pol II crossing the  
62 nucleosomal barrier have not been observed yet. Because the properties of the barrier likely  
63 determine the dynamics of a transcribing polymerase, obtaining high-resolution topographic and  
64 transcriptional maps of the barrier lies at the heart of understanding the regulation of gene  
65 expression.

66 The majority of eukaryotic genes have a well-defined +1 nucleosome (the first nucleosome  
67 encountered by Pol II following initiation), which is enriched in H2A.Z and uH2B histones<sup>5,6</sup>,  
68 and represents the highest barrier to transcription<sup>6</sup>. Whether the high prevalence of H2A.Z and  
69 uH2B modifies the intrinsic barrier at the +1 nucleosome, results in a different local spatial  
70 organization of chromatin, plays a role in regulating the binding and/or activity of extrinsic  
71 transcription factors, or a combination of all of these, remains unknown. Early optical tweezers  
72 studies have shown that in front of a WT nucleosome, Pol II slows down, pauses, backtracks, and  
73 cannot actively ‘peel’ the DNA wrapped around the histones<sup>7</sup>. Instead, the polymerase functions  
74 as a fluctuating ratchet that advances by rectifying transient, spontaneous wrapping/unwrapping  
75 transitions of the nucleosomal DNA around the histone core<sup>7</sup>. A similar study using tailless  
76 histones and mutated DNA sequences suggests that these nucleosomal elements modulate the  
77 topography of the barrier by affecting the density and duration of Pol II pauses<sup>8</sup>. However,  
78 because of their low resolution, these studies failed to accurately map the topography of the  
79 barrier and its effects on the dynamics of transcription. A high-resolution transcriptional map  
80 around the nucleosome is necessary to ultimately understand how the interaction of trans-acting  
81 factors at specific and selective positions of the polymerase around the octamer regulate  
82 transcription across the barrier.

83 Prior attempts to characterize the nucleosomal barrier to transcription have suffered from  
84 two substantial limitations. First, previous assessment of nucleosome stability relied on pulling  
85 and unwrapping the nucleosome from both ends<sup>9</sup>. These experiments, while providing a measure  
86 of the strength of DNA/histone interactions, may not fully recapitulate the physical process of

87 nucleosome invasion by Pol II, which unidirectionally unwinds the nucleosomal DNA. Second,  
88 although we can now obtain transcription trajectories with millisecond temporal and near bp  
89 spatial resolution using optical tweezers<sup>10</sup>, it is very difficult to determine the absolute location  
90 of the polymerase on the template<sup>7,8,11</sup>, what we term here ‘accuracy’. Here we surmount both  
91 limitations, obtaining high-resolution, high-accuracy topographic and transcriptional maps of  
92 WT and modified nucleosomes. By registering the dynamics of Pol II as a function of its position  
93 along the nucleosome, these maps provide a means to interrogate how variant and epigenetically  
94 modified histones affect the dynamics of transcription through the nucleosome.

95

## 96 **Results**

### 97 **Single-molecule Unzipping of Nucleosomal DNA Maps the Topography of the Nucleosome** 98 **Barrier**

99 To experimentally recapitulate the underlying physical process of barrier crossing, i.e.  
100 nucleosomal DNA unwinding, we mimicked the effect of Pol II passage through the nucleosome  
101 using mechanical force. To this end, we adapted a previously described single-molecule DNA  
102 unzipping assay<sup>2,12</sup> in which the two strands of the nucleosomal DNA are held in two optical  
103 traps, resulting in a Y-shaped configuration (Figure 1A). We engineered the stem ahead of the  
104 fork to consist of two consecutive segments of ‘601’ nucleosome positioning sequence (NPS)<sup>13</sup>,  
105 and a short hairpin loop at the end to prevent tether breaking once all double-stranded DNA  
106 (dsDNA) is converted into single-stranded DNA (ssDNA) (Figure 1A). During each experiment,  
107 we move the two traps apart at a constant speed of 20 nm/s. When the force reaches ~ 17 pN, the  
108 dsDNA at the stem begins to unzip. When the stem segment does not contain a nucleosome, the  
109 DNA unzips following a series of closely spaced transitions occurring in a narrow range of  
110 forces between 17 - 20 pN, dictated by the sequence of the template. Once all dsDNA has been  
111 fully converted into ssDNA, the force increases sharply at the hairpin end (Figure 1B). The  
112 highly reproducible force-extension signatures from the two consecutive NPS regions allow us to  
113 align traces from different unzipping experiments by placing the force and dwell-time of the  
114 opening junction at each base pair into register (Figure 1B and S1). Upon force relaxation  
115 (re-zipping), the pattern of closely spaced transitions is reproduced in the inverse sense to that  
116 observed in the pulling direction (Figure 1B, Movie-M1).

117           Next, we repeated the experiment with the second NPS preassembled with a human WT  
118 nucleosome. The unzipping force-extension signature of the first NPS matches those obtained  
119 above, but that of the nucleosome region deviates significantly due to histone-DNA contacts  
120 (Figure 1C and S1A, Movie-M2). Relaxation of the tether results in two identical, sequential  
121 re-zipping signatures characteristic of the naked DNA in ~75% of the cases (Figure 1B and 1C),  
122 indicating that full DNA unzipping led to complete histone removal. However, in 25% of the  
123 cases, when we unzip the same molecule for the second time, the force reaches higher values  
124 than with bare DNA but lower than those observed the first time, likely reflecting residual  
125 histone-DNA interactions from nucleosomal relics. Since we have no knowledge of nucleosome  
126 integrity by the second round of unzipping, we only analyzed the first round of unzipping data  
127 for each molecule. Because we moved the trap at a constant speed, the dwell-time of the fork at  
128 each position reflects the local histone-DNA interaction strength at that force. Indeed, in these  
129 constant pulling velocity experiments, the forces applied to histone-DNA contacts lying deeper  
130 in the structure depend on the forces reached previously in undoing earlier contacts. This effect  
131 may lead to underestimation of the magnitude of later interactions. Accordingly, we also  
132 performed force-jump unzipping experiments on the same constructs in which we suddenly  
133 increased the force to 28 pN (this force was chosen to minimize the contribution of the dsDNA  
134 sequence to the dynamics of the fork) and held it constant while monitoring the unzipping fork  
135 dwell-time at each position along the NPS (Figure 2A). In these experiments, the bare DNA  
136 construct unzips to the hairpin end instantaneously, while the fork dwells in the WT nucleosome  
137 primarily at 25, 31, and 35 bp into the nucleosome (Figure 2B). The residence time histograms of  
138 the unzipping fork along the entire NPS obtained from these two types of experiments are similar  
139 and provide a quantitative description of the barrier to nucleosomal DNA unzipping with single  
140 bp resolution that we term the *nucleosome topography map* (Figure 1E and 2B).

141           The topography maps reveal that the unzipping fork encounters substantial resistance at  
142 around 17, 26, 31, 41, 52, 61 and 69 bp into the nucleosome, which correspond to regions of  
143 proximal dimer and tetramer interaction with the first half of nucleosomal DNA (Figure 1E).  
144 Interestingly, the resistance diminishes significantly after the dyad, suggesting that unzipping the  
145 first half of the nucleosome destabilizes the histone-DNA interactions of the second half. As  
146 previously observed, major histone-DNA interactions first occur ~ 55 bp from the dyad and  
147 exhibit 5 or 10 bp periodicity as the unzipping fork progresses<sup>2,12</sup>. This observation probably

148 reflects the strong histone-DNA contacts along the DNA minor groove every 10 bp observed in  
149 the crystal structure of the nucleosome<sup>14</sup>. Compared to a previous study<sup>2</sup>, we noticed a shorter  
150 residence time near the nucleosome dyad, which we attribute to differences in pulling geometry,  
151 buffer conditions, and/or histone source.

152 Unzipping of tetrasomes (H3/H4 tetramer assembled on NPS) revealed a substantially  
153 diminished barrier compared to the octamer, with unzipping fork dwelling events mostly  
154 restricted to locations near the dyad, and much lower maximum force reached during the  
155 unzipping process (Figure 1E, S1B). These data indicate that the H2A/H2B dimer not only  
156 interacts locally with the DNA but it also affects the strength of the H3/H4 tetramer-DNA  
157 interaction near the dyad to orchestrate the overall nucleosome stability. As loss or exchange of  
158 H2A/H2B dimers has been implicated in important biological processes such as DNA  
159 replication<sup>15</sup>, transcription<sup>16,17</sup>, repair<sup>18</sup>, and DNA supercoiling<sup>19</sup>; these findings highlight the  
160 potential role of non-local histone-DNA interactions in those processes.

161

## 162 **H2A.Z and uH2B Alter Orthogonal Parameters of the Nucleosome Topography Map**

163 Human H2A.Z and uH2B nucleosomes show altered topography maps when compared to their  
164 WT counterparts (Figure 1E and 2B). However, the relative magnitude and distribution of the  
165 peaks are differently affected by these two modifications. Specifically, uH2B nucleosomes  
166 stabilize the dimer region (16 and 25 bp peaks) with minor effects on the tetramer region (Figure  
167 1E and 2B), suggesting that the attachment of ubiquitin to H2B enhances the barrier height  
168 locally. The peaks after the dyad are less pronounced and correspond to regions where  
169 nucleosomal DNA interacts with the distal dimer. H2A.Z nucleosomes show enhanced peaks at  
170 41 and 52 bp, while exhibiting much lower heights at 25 and 31 bp (Figure 1E and 2B),  
171 indicating a global redistribution of the barrier's strength along its width. Overall, in H2A.Z  
172 nucleosomes the dwell-time peaks are more broadly distributed throughout the first half of the  
173 barrier than in their WT or uH2B counterparts, while maintaining their 5 to 10 bp periodicity.

174 To determine whether this redistribution of the barrier strength reflects features of the  
175 individual H2A.Z nucleosomes or the superposition of barriers derived from a heterogeneous  
176 molecular population resulting from an enhanced lateral mobility of these nucleosomes, as has  
177 been previously suggested<sup>12</sup>, we counted the number of transitions (rips) per unzipping trace in  
178 the nucleosome region (Supplementary Methods). Indeed, the H2A.Z-containing nucleosome has

179 on average one more transition per trace than its WT counterpart (Figure S1F) but displays a  
180 similar standard deviation. This effect is also evident in constant force unzipping experiments on  
181 H2A.Z nucleosomes, in which more dwell-time peaks are observed along the NPS (Figure 2B).  
182 To check whether H2A.Z nucleosomes are more mobile compared to WT nucleosomes, we  
183 repeatedly unzipped-rezipped single WT or H2A.Z nucleosomes up to the proximal dimer region  
184 (maximum force reached to ~ 25-30 pN). If H2A.Z induces lateral mobility of the nucleosome,  
185 the position of initial force rise in the nucleosome region would shift between each partial  
186 unzipping-rezipping round, and should be quite evident in our finely registered traces.  
187 Surprisingly, in contrast to the report by Rudnizky et al.<sup>12</sup>, we observed no lateral mobility with  
188 either WT or H2A.Z nucleosomes, as indicated by the highly reversible and overlapping  
189 unzipping signatures in the proximal dimer region (Figure S1G and S1H). Together, these results  
190 indicate that the effect of the H2A.Z histone variant in our experiments is not to increase the  
191 heterogeneity of the nucleosome population but to significantly redistribute the strength of the  
192 barrier, effectively broadening it. This conclusion is also supported by the homogeneous  
193 migration of H2A.Z nucleosomes in native gels. (Figure S1I).

194 The distal dimer interaction peaks for H2A.Z nucleosomes are visibly diminished relative  
195 to those of WT and uH2B nucleosomes (Figure 1E). Interestingly, we observed an increased  
196 cooperativity during the assembly of H2A.Z nucleosomes. As the ratio of octamer to DNA is  
197 increased during nucleosome reconstitution, we consistently observed significantly less  
198 hexasome formation with H2A.Z than with H2A (Figure S2A). It is possible that the global  
199 decrease of DNA interaction with the distal dimer observed with H2A.Z nucleosomes could also  
200 reflect a more cooperative disassembly during unzipping. To pinpoint what regions within  
201 H2A.Z are responsible for its assembly cooperativity, we generated a series of sequence swap  
202 mutants between H2A and H2A.Z (Figure S2B)<sup>20</sup>. Swapping the sequences of the M3 or the M7  
203 region in H2A.Z with the corresponding sequences in H2A promotes the appearance of  
204 hexasomes, indicating decreased cooperativity in assembly (Figure S2A). Consistently, the  
205 topography map of M3\_M7 nucleosomes (an M3 and M7 combined swap mutant) showed  
206 intermediate topographical features between H2A.Z and WT nucleosome, with the distal dimer  
207 interaction peaks (at 109 and 122 bp) becoming more pronounced than those of H2A.Z  
208 nucleosomes (Figure 1E), consistent with the idea that cooperativity in disassembly correlates  
209 with this distal interaction. Structurally the M3 region corresponds to the “loop 1” that mediates

210 H2A.Z-H2A.Z interactions within the octamer, and the M7 region corresponds to the “docking  
211 domain” that mediates H2A.Z interactions with H3-H4<sup>21</sup>. These regions play important roles in  
212 the stability of the histone octamer. Thus, unique physical properties of the H2A.Z octamer  
213 likely account for the broadened barrier distribution we observed during unzipping.

214

### 215 **Observation of Multiple Nucleosomal States at the Proximal Dimer Region**

216 One unique feature from the nucleosome unzipping traces is the presence of fast, reversible  
217 unzipping transitions within the proximal dimer region—spanning the first 40 bp of the NPS—  
218 that manifest as “hopping” of force and extension in the unzipping experiments (Figure S3A).  
219 Hopping in this region is nucleosome-specific, as it is not observed during unzipping of bare  
220 NPS DNA (Figure S3B). Surprisingly, hopping, which is a hallmark of equilibration, was  
221 observed at strand separation rates expected to drive and keep the system out of equilibrium  
222 throughout unzipping. To better capture these hopping dynamics, we fixed the trap distance such  
223 that the unzipping fork remained localized within the proximal dimer region and monitored the  
224 fluctuations of the force and extension (passive mode experiment). Within an empirically  
225 determined trap distance range, we obtained equilibrium extension hopping traces (Figure 3A).  
226 At each fixed trap separation, we determined the number of unzipped bp to obtain a probability  
227 distribution for the length of unzipped DNA (Figure 3B). For both bare and nucleosomal DNA,  
228 these distributions show consistent peaks, as expected on a heterogeneous energy landscape  
229 where the system populates discrete energy wells separated by transition barriers. We note that  
230 certain trap separations allow the system to sample multiple wells, giving rise to a multi-modal  
231 distribution (Figure 3B, bottom panel), analogous to the hopping observed in the constant pulling  
232 rate unzipping curves. Relative to bare DNA, WT nucleosomes display an additional peak in the  
233 distribution of unzipped bps, at approximately 28 bp after the start of the second NPS where the  
234 most significant contacts between DNA and the H2A-H2B dimer occur (Figure 3C). This peak  
235 implies the existence of a barrier to further unzipping that arises from binding of the DNA to  
236 histones, and its position is consistent with the dwell time peak observed in the unzipping traces  
237 (Figure 1E, peak at 26 bp).

238 Assuming that the observed distributions (Figure 3B and 3C) correspond to equilibrium  
239 Boltzmann statistics, we extracted the energy associated with unzipping of each bp in the  
240 proximal dimer region of the nucleosome (Figure 3D, details in Supplementary Methods). The



241 presence of a strong interaction energy peak at 32 bp into the WT nucleosome and the  
242 corresponding energy well preceding this new barrier position account for the appearance of the  
243 new preferred state in the distribution of unzipped bps (Figure 3C, peak at 28 bp). Furthermore,  
244 the low barrier to re-zipping from this state (\* in Figure 3D) implies that the dynamics between  
245 the two states in the proximal dimer region of the nucleosome (at approximately 18 bp and 28 bp)  
246 should be quite rapid, in keeping with the hopping behavior observed in the unzipping curves  
247 (Figure S3A). Subtracting the unzipping energy of bare DNA from that of the nucleosome, we  
248 obtained the additional energy associated with each nucleosome type, providing a measure of the  
249 interaction energy between the DNA and the octamer throughout the first quarter of the NPS  
250 (Figure 3D, inset). WT, H2A.Z, and uH2B nucleosomes all show strong DNA binding to the  
251 proximal dimer region, with a large peak in the interaction energy centered at approximately 35  
252 bp.

253

#### 254 **A “Molecular Ruler” Gauges the Positions of an Elongating Pol II with Near Base-pair** 255 **Accuracy**

256 Having established the topography of the nucleosomal barrier via mechanical force-induced  
257 DNA unwinding, we next set out to determine how this topography manifests in the dynamics of  
258 Pol II during transcription through the nucleosome. We used a high-resolution dual-trap optical  
259 tweezers instrument together with an improved nucleosomal transcription assay (Figure 4). To  
260 accurately gauge the positions of Pol II on the template, we placed a ‘molecular ruler’ in front of  
261 the nucleosome (Figure 4A). The ‘molecular ruler’ consists of eight tandem repeats of an  
262 artificially designed 64-bp DNA that has a single well-defined, sequence-encoded pause site  
263 when transcribed by Pol II in bulk (Figure S4A, dashed rectangle) and in single-molecule assays  
264 (Figure 4B and S4B-D). The repeating pausing patterns of Pol II within the ‘molecular ruler’  
265 generated a periodicity of  $21.1 \pm 0.3$  nm (Figure S4B), corresponding to the length of 64-bp  
266 DNA under experimental force and buffer conditions. This periodicity serves to align all  
267 transcription traces<sup>22,23</sup> and it also enables the accurate conversion of nanometer distances to  
268 basepairs of transcribed DNA (Figure S4D).

269 We used a bubble initiation method to assemble a stalled biotinylated yeast Pol II  
270 elongation complex<sup>7,8</sup> that was ligated downstream to a 2-kb spacer DNA and upstream to the  
271 ‘molecular ruler’, followed by a single nucleosome (Figure 4A). The ‘601’ NPS was used to

272 ensure both precise nucleosome positioning and accurate assignment of Pol II positions as it  
273 crosses the barrier. Pol II transcription was restarted by supplying a saturating concentration of  
274 NTPs (0.5 mM). A Pol II stall site consisting of a short inter-strand cross-linked DNA segment  
275 was placed downstream of the NPS (Figure 4A). In these assays, we used force-feedback to  
276 maintain a constant 10 pN assisting force throughout the transcription trajectory so that the  
277 increase of the distance between the beads serves as an accurate measure of how far Pol II has  
278 transcribed. We find this tethering geometry to be superior to prior designs<sup>7,8</sup> because it isolates  
279 Pol II from the beads surfaces, thus mitigating photo-damage<sup>24</sup>. A representative real-time  
280 trajectory of Pol II transcribing through the ‘molecular ruler’ followed by bare NPS DNA is  
281 shown in Movie-M3.1 and M3.2.

282

### 283 **Real-time, High-resolution Dynamics of Single Pol II Enzymes Transcribing Through** 284 **Single Nucleosomes**

285 We first obtained traces of Pol II transcribing through bare NPS DNA (Figure 5A and 5B, black  
286 trace). Utilizing the pausing patterns obtained with the ‘molecular ruler’ (Figure 4B, inset), we  
287 adapted a recently described algorithm (Gabizon et al., 2018) to align the traces such that the  
288 positions of Pol II along the entire NPS are under registry (Figure 4B and S4D). The results show  
289 that Pol II has a median crossing time within the NPS of 11 s (Figure S6A), a pause free velocity  
290 of  $28.9 \pm 3.0$  nt·s<sup>-1</sup> (Figure S6H), and displays very few backtracking events (0.17 per trace)  
291 (Supplementary file2).

292 Next, we replaced the bare NPS DNA with an assembled *Xenopus* WT (xWT) nucleosome  
293 on the same template (Movie-M4.1 and M4.2). As expected, Pol II exhibits a dramatic slow-  
294 down, with a median crossing time of 129 s (Figure S6B), a pause-free velocity of  $11.4 \pm 4.1$  nt·  
295 s<sup>-1</sup> (Figure S6H), and frequent pausing and backtracking within the NPS region (Figure 4C). 59%  
296 of Pol II succeeded in crossing the barrier (Figure S6F), which is signaled by its reaching the  
297 stall site at the end of the template (Figure 4B). Using the ‘molecular ruler’ to precisely locate  
298 Pol II on the template, and after subtracting the enzyme’s footprint (16 bp)<sup>25</sup>, we obtained a  
299 median dwell-time histogram of the leading edge of Pol II along the entire NPS with  $\pm 3$ -bp  
300 accuracy (depicted as linear and polar plots in Figure 6A). This dwell-time histogram, which we  
301 refer to as a *transcriptional map* of the nucleosome, illustrates at high resolution and accuracy  
302 the height and width of the nucleosome barrier to the elongating Pol II. It complements the

303 topographic map described above, translating it into a “functional map”. Our measurements  
304 represent a nearly 20-fold resolution and accuracy improvement on previous attempts to obtain a  
305 transcriptional map of the nucleosomal barrier, since those experiments could only resolve  
306 roughly three barrier regions of ~50 bp each, corresponding to entry, central and exit zones<sup>7,8,11</sup>.

307 Several features of Pol II barrier crossing dynamics emerge from the nucleosome  
308 transcriptional map (Figure 6A). First, the effect of the barrier begins immediately after the  
309 leading edge of Pol II touches the NPS (3 bp peak); the strength of the barrier is largest at 28 bp  
310 and 10-20 bp before the dyad, and is negligible after crossing this pseudo-symmetry axis. Second,  
311 we identified a region between 28-64 bp into the NPS where Pol II enters long-lived pauses and  
312 backtracks frequently (Figure 4C). These pauses are consistent among different molecules and  
313 exhibit a ~10 bp periodicity (28, 38, 48, 57, and 64 bp into the NPS). Notably, this region  
314 coincides with the region of maximum resistance in the single-molecule unzipping assay (Figure  
315 1E and 2B), implying that the transcriptional barrier encountered by Pol II while crossing the  
316 nucleosome reflects, to a first approximation, the barrier mapped by the unzipping assay. Third,  
317 some molecules were permanently arrested in this region (Figure 5A, B, grey trace), but those  
318 that managed to cross it typically succeeded in reaching the stall site shortly thereafter (Figure  
319 5A). Thus, we speculate that this region (28 – 64 bp) may play an important regulatory role for  
320 barrier crossing by the enzyme. The observed asymmetry of the transcriptional map between  
321 both sides of the dyad axis (Figure 6A) may reflect a substantial weakening of the histone-DNA  
322 interactions in the presence of the bulky resident enzyme halfway across the barrier. However,  
323 the transcriptional map asymmetry is similarly observed in the topographic map (Figure 1E),  
324 even though the bulkiness of the enzyme does not play a role in those experiments. It is also  
325 possible that the barrier asymmetry reflects changes in the nucleosome integrity by the invading  
326 polymerase<sup>17</sup> or the propagating unzipping fork.

327 *Xenopus* histones are traditionally the most-widely used in nucleosome studies because  
328 they are well behaved in recombinant form. Since we employed recombinant human histones in  
329 the unzipping assays, it was of interest to compare the Pol II transcriptional maps of *Xenopus*  
330 nucleosomes with those obtained with their human counterparts utilizing the same 601 NPS. As  
331 seen in Figure 6A, the maps are quite similar except that human nucleosomes confer a  
332 significantly higher barrier to transcription (see Figure 5A-B, Movie-5.1, 5.2 for representative  
333 traces) than those of *Xenopus* in the proximal dimer region (Figure 6A, the 28 bp peak in orange

334 and red panels).

335

### 336 **Dynamic Interplay between Pol II and the Nucleosome During Barrier Crossing**

337 Interestingly, we observed extensive two state transition dynamics while Pol II is paused at  
338 certain sites (frequently at 28 and 63 bp) (Figure 4C, Movie-4.2). While Pol II hopping at 28 bp  
339 coincides with hopping of the unzipping fork near this region and probably reflects sampling of  
340 alternative nucleosomal states ahead of the enzyme, hopping at a much deeper location into the  
341 nucleosome (63 bp) may have a more complex origin. We hypothesize that these latter dynamics  
342 may be due to local Pol II-histone interactions or re-wrapping of the nucleosome in front of a  
343 backtracked enzyme. Indeed, these hopping dynamics occur exclusively after Pol II enters a  
344 deeply backtracked state (Figure S5).

345 We also investigated whether Pol II remains functionally competent after the crossing. The  
346 pause-free velocity of Pol II after exiting the nucleosome resumed to 70 % ( $28.6 \pm 0.8 \text{ nt}\cdot\text{s}^{-1}$ ) of  
347 its value before the crossing ( $41.1 \pm 1.0 \text{ nt}\cdot\text{s}^{-1}$ ). This observation seems to indicate that while the  
348 enzyme remains functionally competent, its dynamic state has been affected by the encounter  
349 (Figure S6H). It remains unknown what changes in the enzyme are responsible for this slowing  
350 down and if they are reversible. On the other hand, we probed the integrity of the nucleosome by  
351 pulling away the two beads after Pol II crossed the barrier. If the nucleosome survived the  
352 traversal by Pol II, it would now lie between the two tethering points, i.e. the upstream DNA  
353 handle and the polymerase. Rarely ( $< 5\%$ ) these pulling curves displayed the force-extension  
354 signature normally associated with the presence of a nucleosome, suggesting that *in situ*  
355 reassembly of the nucleosome following Pol II traversal was inefficient under our assay  
356 conditions. A similar low efficiency of nucleosome reassembly was observed from transcription  
357 assays in bulk in the absence of factors added in trans such as FACT (facilitates chromatin  
358 transcription)<sup>26</sup>.

359

### 360 **H2A.Z Enhances the Width and uH2B the Height of the Transcriptional Barrier**

361 Next, we investigated the effects of human H2A.Z and uH2B on Pol II transcription  
362 dynamics. Our unzipping assay revealed that H2A.Z and uH2B have distinct effects on the  
363 nucleosome barriers (Figure 1E and 2B). Under the same buffer and force conditions, Pol II  
364 alone was capable of crossing either H2A.Z (Figure 5C and 5D, Movie-M6.1 and M6.2) or

365 uH2B (Figure 5E and 5F, Movie-M7.1 and M7.2) nucleosomes. While the crossing probabilities  
366 of Pol II through H2A.Z and WT nucleosomes are similar (58% and 59%, respectively) (Figure  
367 S6F), the distributions of pause sites within the NPS are markedly different (Figure 6A) in that  
368 H2A.Z is seen to cause a global redistribution of Pol II pause sites along the entire NPS. Such  
369 scattered distribution (3, 28, 36, 59, 66, 87, 101, 115, 125 and 138 bp) differs significantly from  
370 that of WT nucleosome (3, 28, 57, 64 bp) where most pauses occur before the dyad. This  
371 spreading of the barriers for H2A.Z nucleosomes is a further indication that the force applied to  
372 the upstream DNA (which is the same in both experiments) is not the dominant factor  
373 responsible of the asymmetry of the WT barrier across the dyad, but that the actual histone-DNA  
374 interactions are. Furthermore, these differences are unlikely to stem from H2A.Z nucleosomes  
375 being mis-positioned on the starting template, because the first pause site at  $\sim 3$  bp, where the  
376 leading edge of Pol II begins to interact with the nucleosome, is observed in every molecular  
377 trajectory obtained with H2A.Z nucleosomes. Instead, we attribute them to broadened  
378 distributions of DNA-histone interactions as seen in the topography map for H2A.Z nucleosomes  
379 (Figure 1E and 2B, also see discussion on energetic profiles of H2A.Z nucleosome in next  
380 section). Clearly, H2A.Z strongly modulates the width of the nucleosomal barrier to transcription.

381 In contrast, Pol II transcription through human uH2B nucleosomes has a slightly higher  
382 passage probability (76%) than through hWT nucleosomes (Figure S6F), although at the expense  
383 of longer crossing times (Figure S6E). The pause site distribution also resembles that of the hWT  
384 or the xWT nucleosomes (Figure 6A), however, the median dwell-time of Pol II at pause sites  
385 near the dyad is more than double that for the WT nucleosome, suggesting that uH2B enhanced  
386 the height of the nucleosomal barrier to Pol II (Figure 6A). The overall pause-free velocities of  
387 Pol II transcription through H2A.Z ( $11.4 \pm 7.1$  nt-s<sup>-1</sup>) and uH2B nucleosomes ( $12.9 \pm 3.4$  nt-s<sup>-1</sup>)  
388 are lower than that through hWT ( $18.2 \pm 7.1$  nt-s<sup>-1</sup>) nucleosomes (Figure S6H). Consequently,  
389 the median crossing times of Pol II through H2A.Z (262 s) and uH2B (304 s) nucleosomes are  
390 longer than that through hWT nucleosomes (230 s) (Figure S6C-E). Note, however, that pause-  
391 free velocity contributes negligibly to crossing time, as the latter is dominated by long pauses.  
392 Including pausing, translocation and backtracking, Pol II takes longer to cross uH2B or H2A.Z  
393 than hWT nucleosomes (Figure 6B).

394 Similar to when traversing hWT nucleosomes, Pol II backtracks frequently during  
395 transcription through H2A.Z and uH2B nucleosomes (Figure S5A, S5C and S5E). The average

396 number of backtracks and backtrack depths are similar, but backtrack durations are longer when  
397 Pol II transcribes through H2A.Z nucleosomes than through WT and uH2B counterparts  
398 (Supplementary file2), which may again reflect the broader extent of histone-DNA interactions  
399 in H2A.Z nucleosomes. Failure to recover from some backtracks seems to contribute to Pol II  
400 arrests, the positions of which were more scattered for Pol II transcribing through uH2B and  
401 H2A.Z than through WT nucleosomes (Figure S6G). Interestingly, backtracked Pol II frequently  
402 enters long-lived pauses, some of which are also accompanied by frequent two-state transition  
403 dynamics (hopping behavior) (Figure S5D and S5F). During some of the long-lived pauses  
404 associated with crossing of uH2B nucleosomes, we also observed three-state hopping behavior  
405 (Figure S5F) and large hopping transition events (Figure 5F, green trace) of Pol II. As this  
406 behavior is rarely observed in WT and H2A.Z traces (Figure 5), we speculate that these  
407 dynamics of Pol II reflect the presence of the bulky ubiquitin attachment. Collectively, these data  
408 reveal that H2A.Z mainly enhances the width and uH2B mainly enhances the height of  
409 nucleosomal barrier to transcription. Consistent with the previously reported higher stability of  
410 uH2B nucleosomes<sup>27,28</sup>, they pose an overall higher barrier magnitude—especially in the region  
411 near the dyad—than their WT counterparts to the passage of polymerase. It is also worth noting  
412 that for WT and H2A.Z, but not for uH2B nucleosomes, the transcriptional map replicates the  
413 corresponding topography map, suggesting that there could be uH2B-Pol II specific interactions  
414 that are not present in the unzipping assay.

415 Our findings provide direct evidence that H2A.Z or uH2B by themselves affect the  
416 crossing dynamics of Pol II; and despite their differential effects on nucleosome topography,  
417 they both represent stronger barriers than WT nucleosomes for Pol II.

418

### 419 **A Mechanical Model for Pol II Transcription Through the Nucleosome**

420 We use a simplified mechanical model to calculate the expected polymerase dwell times along  
421 nucleosomal DNA given a profile of DNA-octamer interaction energies. We build on a  
422 previously published Pol II model that includes a mechanical DNA linkage between Pol II and  
423 the nucleosome, in addition to nucleosome-Pol II steric interactions (Figure 7A)<sup>29</sup>. The model  
424 assumes that Pol II is unable to actively separate the DNA from the surface of the octamer.  
425 Instead, the enzyme behaves as a ratchet that makes progress by rectifying the unwrapping  
426 fluctuations of the nucleosomal DNA. The enzyme can also backtrack and diffuse forward to re-

427 engage the 3'-end of the nascent transcript with its active site. The extended model incorporates  
428 varying binding energies for the DNA along the nucleosome.

429 Polymerase progress along the nucleosomal DNA is modeled as a series of transcription  
430 steps and backtracking excursions (Figure 7B), adapting the model of Dangkulwanich et al.<sup>30</sup> to  
431 include interactions with the nucleosome. The individual polymerase steps are assumed to occur  
432 on an energy landscape that encompasses both the elastic energy of deforming the unwrapped  
433 DNA linker between Pol II and the nucleosome core particle, and the interaction energy between  
434 the wrapped DNA and the core particle (Figure 7C). For a given Pol II position, the amount of  
435 unwrapped DNA is assumed to fluctuate rapidly around an energy minimum that balances these  
436 two contributions. As Pol II steps forward, the linker shortens and the elastic energy increases,  
437 with a longer linker entailing a smaller energy increase and thus a more rapid rate constant for  
438 polymerase forward motion. The interaction energy profile between the DNA and the histone  
439 octamer ahead of Pol II determines the ensemble of linker lengths and, thus, indirectly controls  
440 the average time spent by Pol II at each DNA base pair. This model allows us to calculate the  
441 expected dwell time of the polymerase at each position.

442 Accordingly, we use the DNA-octamer interaction energies extracted from equilibrium  
443 unzipping data (Figure 3D) to calculate the expected mean dwell times of polymerase in the  
444 proximal nucleosomal region. The dwell time peaks resulting from these equilibrium interaction  
445 energies approximately correspond to peaks in the experimental dwell time profiles (Figure S7).  
446 The DNA-octamer interaction energies cannot account for the first dwell time peak (the peak at  
447 ~3 bp in Figure 6A) corresponding to the initial encounter between Pol II and the nucleosome.  
448 We hypothesize that this peak is the result of additional interactions between Pol II and the  
449 histone proteins rather than arising from the difficulty of peeling DNA from the nucleosome.

450 Because equilibrium interaction energy data was available only for the initial section of the  
451 nucleosome (Figure 3), Pol II dwell times further into the nucleosomal sequence cannot be  
452 predicted from the data available. Instead, we solve the inverse problem: given the measured Pol  
453 II mean dwell times (Figure 7D), we fit the DNA-nucleosome interaction energies (Figure 7E)  
454 required to generate this dwell time profile (Supplementary Methods). The dependence of dwell  
455 times on the nucleosome binding energy in this model is non-local—time spent at a particular bp  
456 depends on the energy required to unwrap a segment of DNA *ahead* of the polymerase.  
457 Consequently, peaks in the dwell time profile arise from interactions that involve both large

458 energy values and span a substantial length of DNA (extended regions of strong binding). For  
459 example, the peaks at 29 bp in the dwell time profiles for hWT, uH2B, and H2A.Z nucleosomes  
460 (Figure 7D), correspond to large peaks in the interaction energy at 32 bp, consistent with the  
461 interaction energy profiles obtained from equilibrium DNA unzipping data (Figures 3D). A two-  
462 peaked region of strong binding at roughly 43 bp in the H2A.Z and uH2B nucleosomes gives rise  
463 to corresponding double peaks in the dwell time profiles 41 bp into the nucleosomes, with  
464 substantially longer pausing times for H2A.Z nucleosomes in this region. An additional broad  
465 region of strong binding is seen just before the dyad axis, 62 bp in hWT and uH2B nucleosomes,  
466 resulting in the observed Pol II pausing peaks 59 bp into the nucleosome. Interestingly,  
467 according to our mechanical model, the predicted interaction energies necessary to generate the  
468 observed dwell-time profiles are similar in magnitude for all three nucleosomal types. However,  
469 wider peaks of strong binding give rise to increased pause durations in the uH2B transcriptional  
470 profile, while a distribution of many narrower peaks accounts for the increased number of  
471 pausing sites in the H2A.Z profile (Figure 7D, E).

472

## 473 **Discussion**

474 For the last 20 years the crystal structure of the nucleosome<sup>14</sup> has guided our view of the  
475 packaging unit of the genome and suggested its role as a regulator of gene expression. As a  
476 mechanical and energetic barrier, the nucleosome gates the accessibility of genomic DNA,  
477 constituting a fundamental regulatory mechanism for all DNA-templated processes including  
478 replication, transcription, repair, recombination, and chromatin remodeling. Epigenetic  
479 modifications and histone variants are known to modulate all of these processes. The question of  
480 whether this modulation results from the recruitment of trans-acting factors, or responds to  
481 changes in the intrinsic properties of the barrier, or both, has not previously been addressed.

482 Low-resolution single molecule assays showed that it is possible to follow molecules of  
483 Pol II as they cross the nucleosomal barrier<sup>7,8</sup>. However, these studies only yielded gross features  
484 of the barrier and failed to provide the crucial spatial-dependent dynamics of the crossing that are  
485 required to rationalize the effect of nucleosome modifications at the molecular level.

486 Very recently, cryo-EM structures of Pol II-nucleosome complexes have provided  
487 snapshots of Pol II paused at major histone-DNA contacts and suggested sites of interaction with



488 other factors<sup>31-33</sup>. Missing from these structures is information about the dynamics of barrier  
489 crossing by the enzyme: what are the time windows available for in-trans interactions with these  
490 discrete sites, how are these related to the local energetic magnitude of the barrier, and how are  
491 they modulated by epigenetic modifications and histone variants. Using a ‘molecular ruler’, we  
492 have been able to locate individual Pol II molecules along the template with high precision and  
493 to extract their molecular trajectories as they transcribe through nucleosomes at near bp  
494 resolution and accuracy. These trajectories unveil unprecedented details on the general dynamics  
495 (translocating, pausing, hopping and backtracking) as well as the residence times of the enzyme  
496 at every position as it progresses through the nucleosome, providing insights into how gene  
497 expression is regulated spatially and temporally at a single nucleosome level.

498 Our results reveal that the proximal dimer region of the nucleosome (~28 bp) in the  
499 transcription direction is a major physical barrier for Pol II and may serve as an important  
500 regulatory checkpoint for gene expression. In this region, Pol II frequently enters long-lived  
501 pauses; this result is consistent with the observation of a major Pol II pause site at the  
502 superhelical location SHL(-5) reported recently<sup>32</sup>. Interestingly, pausing at this location is  
503 accompanied by extensive hopping dynamics, likely reflecting unwrapping/rewrapping of the  
504 nucleosomal DNA around the octamer and/or structural rearrangements of the nucleosome.  
505 Indeed, partially unwrapped nucleosomal intermediates have been detected *in vitro* by time-  
506 resolved small angle X-ray scattering<sup>34</sup>, by cryo-EM<sup>35</sup> and *in vivo* by MNase-seq<sup>16</sup>. The location  
507 of these structural intermediates coincides with the different nucleosomal hopping states  
508 observed as the unzipping fork reaches the proximal dimer, reinforcing the interpretation that  
509 local DNA/histone interactions determine the dynamics of Pol II in this region and its ultimate  
510 progress beyond it.

511 Traditionally, the dyad has been viewed as the strongest histone-DNA contact point and  
512 therefore as the highest barrier position in WT nucleosomes. Unambiguously assigning Pol II’s  
513 residence time with bp resolution has allowed us to define a transcriptional map of the barrier,  
514 which indicates that the proximal dimer region and not the dyad represents the highest barrier to  
515 an elongating Pol II. This observation is consistent with the unzipping experiments that also  
516 reveal the proximal dimer region as mechanically the most stable. We posit here that the change  
517 in dynamics of the polymerase, progressing slowly in this region, provides a crucial time window  
518 to allow for other facilitative or inhibitory factors to bind and further modulate the strength of the

519 barrier to the transcribing enzyme. For instance, FACT may bind to the nucleosome and remove  
520 one histone dimer ahead of the Pol II and reassemble the nucleosome after Pol II traversal.<sup>36–38</sup>.  
521 These early regulatory steps as Pol II invades the nucleosome not only gate gene expression but  
522 also permit the regulation of chromatin integrity and of epigenetic modifications. As Pol II  
523 progresses further into the nucleosome, the strength of the barrier appears to be dynamically  
524 modified either through nucleosome destabilization, the steric bulkiness of the enzyme, or both.  
525 Beyond the dyad, there is practically no barrier in WT nucleosomes, again in agreement with a  
526 recent cryo-EM structural report<sup>32</sup>.

527 Consistent with these observations, modifications that play important regulatory roles such  
528 as H2A.Z and uH2B, mainly affect the proximal dimer region, although their effects are not  
529 circumscribed to this location. Pol II transcription through nucleosomes bearing H2A.Z or uH2B  
530 reveal that these modifications strongly increase the strength of the barrier, but do so  
531 distinctively: H2A.Z increases the width of the barrier whereas uH2B increases its height.  
532 Significantly, the topographic map of the WT and H2A.Z barriers before the dyad, as determined  
533 here by force-induced nucleosomal DNA unwinding, closely parallels the transcriptional map of  
534 Pol II, indicating that to a first approximation, the ability of the enzyme to cross the barriers in  
535 this region is dictated by the energetic requirements of disrupting DNA-histone interactions.

536 *In vitro*, H2A.Z has been observed to either enhance or decrease nucleosome stability  
537 depending on the assays used<sup>21,39</sup>. Our improved optical tweezers experiments offer  
538 unprecedented resolution that captures a more complex picture in which H2A.Z redistributes the  
539 strength of the barrier across and beyond the dyad, effectively increasing its width. Accordingly,  
540 the physical barriers across the H2A.Z nucleosome are lower, yet more globally distributed. The  
541 precise origin of this broader distribution is not known. A previous study suggested that H2A.Z  
542 nucleosomes are more mobile compared to their WT counterparts, although the extent and cause  
543 of the mobility remain unclear<sup>12</sup>; however, we do not observe this enhanced mobility in our  
544 experiments. Like a previous study<sup>40</sup>, our data support the idea that the H2A.Z octamer is more  
545 stable than its WT counterpart within the nucleosome. As a result, H2A.Z hexasomes are barely  
546 observed during nucleosome assembly and we find that the M3 and M7 regions within H2A.Z  
547 are important for conferring such increased octamer stability. We speculate that increased  
548 octamer stability strengthens the overall nucleosomal barrier as reflected in the increased  
549 crossing time of Pol II through such nucleosomes.

550 The effect of H2A.Z on the nucleosomal barrier can be seen as that of re-distributing the  
551 strength of the barrier from height to width. Interestingly, the Arrhenius dependence of barrier  
552 crossing time predicts that the time to cross a barrier of height  $n \times h$  is proportional to the  $n$ th-  
553 power of the time to cross a barrier of height  $h$ . In contrast the time to cross  $n$  sequential barriers  
554 of height  $h$  is proportional to  $n$  times the time to cross each one of the barriers. Thus, based on  
555 these considerations alone, we would expect that H2A.Z would decrease the crossing time of  
556 Pol II, not increase it, as observed. Therefore, factors other than barrier crossing time, but  
557 favored by the presence of the barrier (e.g. backtracking, pausing, etc), are the ones that  
558 dominate the overall crossing time in the case of H2A.Z nucleosomes. By dividing the height of  
559 the barrier into several smaller ones, H2A.Z nucleosomes provides the enzyme more  
560 opportunities at different locations to pause, backtrack and possibly interact with regulatory  
561 factors acting in trans such as chaperones and chromatin remodelers. In vivo, the effects of  
562 H2A.Z on transcription are complex and somewhat species-dependent. The strong barrier posed  
563 by H2A.Z nucleosomes may explain its role in poisoning quiescent genes for activation in yeast<sup>41</sup>  
564 and its prevalence in +1 nucleosomes across eukaryotic genomes<sup>4</sup>. In contrast, the observation  
565 that H2A.Z facilitates transcription in multi-cellular organisms<sup>4</sup> is more likely due to recruitment  
566 of trans-acting factors.

567 Using homogeneous, chemically-defined recombinant nucleosomes, we also demonstrated  
568 that uH2B strengthens histone-DNA interactions at the dimer region and increases the overall  
569 barrier strength to Pol II. Interestingly, while uH2B occurs at the dimer region, its effect on Pol II  
570 transcription propagates to other regions of the nucleosome including the region preceding the  
571 dyad. Thus, the effects of epigenetic modifications are not merely local but may extend further  
572 into the barrier. Uncovering such position-dependent nucleosome properties and dynamics has  
573 been possible by the high resolution and accuracy achieved in our single-molecule assays.

574 *In vivo*, H2B ubiquitination is highly dynamic and both the addition and removal of  
575 ubiquitin are required for optimal transcription<sup>42</sup>. Like H2A.Z, it is not known whether these  
576 phenotypes are due to altered nucleosome stability or to impaired or facilitated recruitment of  
577 trans-acting factors. Nevertheless, higher levels of H2A.Z and uH2B are observed in  
578 transcriptionally silent gene promoters in yeast<sup>27,43</sup>. Preventing H2B ubiquitination in yeast led to  
579 increased Pol II occupancy and transcription from quiescent promoters<sup>27</sup>. These observations are  
580 consistent with our data that H2A.Z and uH2B provide orthogonal and selective means to

581 enhance the transcription barrier thus contributing to the maintenance of the transcriptional  
582 ground state and to gene silencing. Our results show that while these modifications may also act  
583 indirectly through their actions on the binding of trans-acting factors, they exert a direct and  
584 significant effect on transcription dynamics by Pol II.

585 We have developed a unified mechanical model that uses the experimentally determined  
586 space-resolved residence times of the enzyme at each position on the nucleosome to determine  
587 the energetics of the barrier. This model is quite general and should prove useful in predicting  
588 the behavior of Pol II through alternative barriers, and in understanding the mechanics of barrier  
589 crossing for other molecular motors.

590 The dynamics of Pol II transcription through the nucleosome *in vivo* are affected by  
591 numerous other factors such as higher-order chromatin folding, DNA topology, and transcription  
592 regulators including histone chaperones, elongation factors, and chromatin remodelers.  
593 Integrating one or more of these elements in single-molecule assays such as the one presented  
594 here provides an interesting avenue for future work to fully elucidate the features and principles  
595 underlying this biologically crucial and biophysically complex molecular encounter. Because  
596 epigenetic modifications are potent regulators of eukaryotic gene expression, these results shed  
597 new light on the mechanistic link between modifications enriched on the +1 nucleosome and the  
598 barrier to transcription. More broadly, the real-time characterization of the dynamics of Pol II  
599 molecules traversing through nucleosomes at the highest resolution and accuracy reported so far,  
600 and the resulting nucleosome transcriptional map, constitute important steps towards uncovering  
601 the physical mechanisms underpinning the regulation of eukaryotic gene expression.

602

## 603 **Methods**

### 604 **General materials**

605 All DNA modifying enzymes were purchased from New England Biolabs (NEB). Oligonucleotides were  
606 purchased from Integrated DNA Technology (IDT). Nucleotide triphosphates were purchased from Thermo  
607 Scientific, and standard salts and buffer components were purchased from Sigma Aldrich. Cloning and DNA  
608 template construction follows standard molecular biology techniques unless otherwise noted. The sequences of  
609 all oligos used are listed in Supplementary file 1.

610



## 644 **Histone octamer assembly and purification**

645 Recombinant human histones H2A, H2B, H3.3 and H4 were purchased from the Protein Expression and  
646 Purification (PEP) Facility at Colorado State University. H2A.Z, H2A/H2A.Z swap mutants and all *Xenopus*  
647 *laevis* histones were expressed in *E. coli*, purified and reconstituted into octamers according to standard  
648 protocols<sup>44</sup>. uH2B was prepared by crosslinking ubiquitin (G76C) and H2B (K120C) as previously described<sup>45</sup>.

## 649 **Nucleosome reconstitution on NPS-hp**

650 Purified human histone octamers or tetramers were stored in 10 mM Tris, pH 7.6, 1.6 M NaCl, 1 mM EDTA, 1  
651 mM DTT, 20% glycerol at -80°C. The reconstitution of nucleosome was performed using a salt dilution  
652 method as described<sup>44</sup>. Briefly, NPS-hp DNA and histone octamers or tetramers were mixed in different molar  
653 ratios ranging from 1:0.8 to 1:1.4 and initial salt concentration of the mixture (10  $\mu$ L) was brought to 2 M  
654 NaCl. These reactions were incubated at 30 °C in a PCR machine and the following amounts of dilution buffer  
655 (10 mM Tris, pH 7.6, 1 mM EDTA, 1 mM DTT, 0.1 mg/mL BSA) were added every 15 min: 3.3, 6.7 5, 3.6,  
656 4.7, 6.7, 10, 30, 20, 100  $\mu$ L. The reaction products were analyzed by native polyacrylamide gel electrophoresis  
657 (4%, acrylamide:bisacrylamide ratio 37.5:1) with 0.5  $\times$  TBE plus 5 mM MgCl<sub>2</sub> on ice. The reaction that gave  
658 no aggregates and minimal amounts of free DNA was chosen for further concentration using Amicon Ultra  
659 centrifugation filters with Ultracel 100K membrane. Concentrated nucleosomes were supplemented with 0.02 %  
660 NP40 and stored at 4 °C.

## 661 **Optical tweezers assay for single-molecule unzipping**

662 Unzipping oligo beads were prepared by ligating 5'-CGGT 1  $\mu$ m polystyrene oligo beads with Y-alignment  
663 DNA, NPS-hp nucleosome (or NPS-hp DNA) using *E. Coli* DNA ligase. The reaction was carried out at 16 °C  
664 for 2-3 hours. The ligated beads were diluted with TB50 buffer (20 mM Tris, pH 8.0, 50 mM KCl, 5 mM  
665 MgCl<sub>2</sub>, 1 mM DTT, 10 mM NaN<sub>3</sub>, 0.1 mg/mL BSA) to a final bead density of 0.00006% (w/v) and loaded into  
666 the tweezing chamber, which was filled with TB50 buffer. Tweezing chamber was pretreated with 5% Pluronic  
667 F-127 and 1 mg/mL BSA followed by washing with TB50 buffer prior to each experiment. The 1.26  $\mu$ m SA  
668 beads were diluted directed with TB50 buffer to the same bead density as that of oligo beads.

669 Optical tweezers experiments were performed in a custom-made dual-trap optical tweezers instrument  
670 modified from the design in Comstock et al<sup>46,47</sup>. In this configuration, a 1064 nm laser is passed through an  
671 acousto-optic deflector, with the laser alternating in position between the two traps every 5  $\mu$ s. The position of  
672 the beads relative to the traps was measured using back focal plane interferometry<sup>48</sup>. Single tethers were  
673 formed in situ inside the chamber by trapping an oligo bead in one trap and an SA bead in the second trap, and  
674 bringing in close proximity the two traps to allow the biotin on the right arm of the Y to interact with  
675 streptavidin (Streptavidin bead).

## 676 **Unzipping at a constant trap separation speed**

677 Once a single tether was confirmed, the trap distance was reset to a value at which the tether force was ~ 0.4  
678 pN. Unzipping was initiated by moving the two traps apart at a constant speed of 20 nm/s for a total of 875 nm.  
679 Reziping was conducted at the end of unzipping by bringing the two traps together to the initial trap position  
680 at the same speed. The tether was broken manually by increasing the trap distance and calibration was  
681 performed as previously described<sup>49</sup>. Data was acquired at 800 Hz.

## 682 **Unzipping at 28 pN constant force**

683 To unzip the construct at constant force, the tether was initially held at ~ 10 pN and force feedback was turned  
684 on to maintain the tether at a constant force of 28 pN. The position and distance between the two beads were  
685 recorded at 800 Hz until the construct was fully unzipped. The force feedback was turned off and the tether  
686 was relaxed to ~ 0.5 pN. For the purpose of aligning the traces and accurately converting nanometer distance  
687 to basepairs unzipped, an unzipped trace using constant trap separation speed (as described above) was further  
688 obtained from the same tether.

## 689 **Partial unzipping up to the proximal dimer region to test nucleosome mobility**

690 Unzipping was performed at constant trap separation speed of 50 nm/s up to the proximal dimer region where  
691 the force starts to rise above the baseline of bare DNA construct, but does not reach 30 pN. The partial  
692 unzipping was followed by reziping to the initial trap position. Typically, this results in a trap movement of ~  
693 620 nm. After repeating the unzipping-reziping cycle for 5 -10 times, a final unzipping that unzips all the way  
694 to the hairpin end (trap movement of 875 nm) was performed to disrupt the whole nucleosome. A bare DNA  
695 trace was also collected immediately following this final unzipping.

## 696 **Unzipping at constant trap distances to record hopping traces near the proximal dimer 697 interaction region**

698 To capture hopping of the unzipping fork near the proximal dimer interaction region of the nucleosome, the  
699 trap was manually moved apart at a small distance increment of 7.1 nm. At each discrete trap position (passive  
700 mode), the distance between the two beads was recorded at 2.5 kHz for 10-300 seconds. Initially, only fast  
701 hopping events characteristic of dsDNA unwinding were present. Once the unzipping fork arrived at the  
702 proximal dimer interaction of the nucleosome, additional slow transition events, due to histones binding with  
703 and dissociating from dsDNA or ssDNA, could be seen. Recording was terminated when the force reached ~  
704 23 pN. The tether was then relaxed to ~ 0.5 pN. For the purpose of aligning the traces and accurately  
705 converting nanometer distance to basepairs unzipped, an unzipped trace using constant trap separation speed  
706 (as described above) was further obtained from the same tether.

## 707 **Construction of the 8 × repeat ‘molecular ruler’ plasmid**

708 The plasmid that contains a single repeat sequence (pGEM3z-1×repeat) was first cloned by modifying a  
709 pGEM3z-T7A1 plasmid<sup>22</sup>. The construction of the plasmid with eight tandem repeat sequences (pGEM3z-  
710 8×repeat) was carried out by following a published protocol<sup>50</sup> using BglII, DraIII and EagI restriction sites. This  
711 method allows doubling of the repeat number following each cycle of cloning. To ease isolation and  
712 purification of the 8 × repeat DNA for future ligation steps, we removed the internal BsaI site in pGEM3z-  
713 8×repeat and introduced two BsaI sites flanking the 8 × repeat region by using an overlap PCR strategy.  
714 Briefly, two fragments outside the 8 × repeat region of the plasmid were amplified using oligos ZC12-ZC13  
715 and ZC14-ZC15, respectively, and assembled into one fragment using ZC12-ZC15. The assembled fragment,  
716 which is devoid of the internal BsaI site, was digested with SapI/EagI and ligated with SapI/EagI digested 8 ×  
717 repeat fragment from pGM3z-8×repeat. The resulting plasmid pGM3z-8×repeat-2×BsaI contains the 8 × repeat  
718 sequence flanking by two BsaI sites, which are included in oligos ZC12 and ZC15. All plasmids containing  
719 repeat sequences were transformed and grew in SURE2 competent cells at 30 °C. Large amounts of pGM3z-  
720 8×repeat-2×BsaI plasmids were purified from 150 mL of SURE2 cells using Zyppy™ Plasmid Maxiprep Kit.

## 721 **DNA templates for Pol II nucleosomal transcription assay**

722 The 8 × repeat DNA with proper overhangs were digested from pGM3z-8×repeat-2×BsaI using BsaI-HF and  
723 purified using 8 % native PAGE.

724 The crosslinked DNA (XLink) used to stall Pol II at the end of the template was prepared by  
725 annealing ZC16 and ZC17. The annealed oligos were diluted to 1 μM in TE with 20% DMSO and 50 μM  
726 trioxsalen, irradiated by 340 nm UV light for 15 minutes. Extra trioxsalen (10 μM more) was added and the  
727 oligos were irradiated for another 15 minutes. This procedure was repeated to ensure complete crosslinking.  
728 The crosslinked oligos were bound to 1 mL HiTrap Q column (GE Healthcare), washed with 4 mL TE buffer,  
729 then 4 ml TE buffer + 250 mM NaCl, eluted with TE + 1 M NaCl, and desalted using Amicon Ultra  
730 centrifugation filters with Ultracel 3K membrane. The sequences of the crosslinked oligos are:

731 5' phos-GGTGTACAGAACGCAATGAATT 3'

732 3' GGACCACATGTCTTGCGTTACTTAA 5'

733 NPS DNA (308 bp) that contains the 147 bp ‘601’ NPS was amplified from a pGMZ-3z/601 plasmid  
734 using oligos ZC18 and ZC19. The NPS DNA was digested with BsaI/DraIII, purified using HiTrap Q column,  
735 and ligated to the crosslinked oligo. The ligation product (NPS-Xlink) was purified using 8 % native PAGE.

736 The 2 kb upstream spacer DNA and 1.5 kb biotin handle DNA were amplified from lambda DNA  
737 using oligos ZC20-ZC21, ZC22-ZC23, respectively. PCR products were digested with BsaI and purified using  
738 1% agarose gel. Both the 2 kb spacer and 1.5 kb biotin handle DNA were ligated to 5'-CGGT 1 μm  
739 polystyrene oligo beads overnight at 16 °C using T4 DNA ligase (NEB). The ligated beads were first washed  
740 with TE + 0.5 M KCl + 20 μg/mL β-casein, then washed twice with TE + 20 μg/mL β-casein and resuspended



741 in TE + 20  $\mu\text{g/mL}$   $\beta$ -casein to a concentration of 0.02% (w/v) for 1.5 kb biotin handle, and 0.2 % (w/v) for 2  
742 kb spacer DNA. The ligated beads were stored at 4 °C until experiments.

### 743 **Assembly of yeast Pol II stalled complex**

744 Biotinylated yeast Pol II holoenzyme was expressed, purified and biotinylated as previously described<sup>51</sup> and  
745 was a generous gift of Prof. Craig Kaplan. The stalled Pol II elongation complex was prepared by a bubble  
746 initiation method followed by uridine triphosphate (UTP) starvation<sup>7</sup>. The sequences for the template DNA  
747 strand (TDS), non-template DNA strand (NDS) and short RNA (RNA9) are:

748 *NDS*:

749 5' AGGTCTCAGAAGACGCCCGAACAAACAGACACAAACACCACGGCCGGCGAGCCAGACACGACC  
750 AATTATCTATGTA~~ACTT~~GCCATATTCAGGATTAT 3'

751 *RNA9*:

752 5' GACGCCCGA 3'

753 *TDS*:

754 3' TCCAGAGTCTTCTGCGGGCTTGTGTCTGTGTTTGTGGTGCCGGCCGCTCGGTCTGTGCTGGTTA  
755 ATAGATACATTGAACGGTATAAGTCCTAATAGTCA-phos 5'

756 To assemble the stalled complex, TDS was incubated with RNA9, heated to 45 °C and cooled down to  
757 20 °C at 1 °C/min to form the TDS/RNA9 hybrid. Pol II was added to the hybrid and incubated at room  
758 temperature (RT) for 10 min, followed by NDS addition and incubation at 37 °C for 15 min. Transcription was  
759 initiated by adding ATP/GTP/CTP to a final concentration of 10  $\mu\text{M}$  each and the reaction was incubated at  
760 RT for 10 min. If Pol II succeeded in restarting, it will be stalled at the first A site on TDS (bolded and  
761 underlined in the sequence above) due to absence of UTP. The relocation of Pol II to the stall site will also  
762 expose a BsaI site (underlined above) shielded initially by Pol II and only those complexes in which Pol II  
763 succeeded in restarting can be digested and further ligated to the 2 kb upstream spacer. The stalled complex  
764 was digested with BsaI-HF at 37 °C for 15 min, aliquoted, and stored at -80 °C until usage.

### 765 **Nucleosome reconstitution on NPS-Xlink template**

766 *Xenopus* WT (xWT) nucleosome was reconstituted by salt-dialysis using NPS-Xlink DNA with *Xenopus*  
767 *laevis* recombinant histone octamer. Human WT (hWT), uH2B and H2A.Z nucleosomes were reconstituted  
768 similarly to those used in the single-molecule unzipping assay, except that NPS-Xlink DNA was used. The  
769 efficiency of nucleosome reconstitution was assessed by 4% native PAGE. In case where a significant amount  
770 of free DNA was present, the nucleosome was further purified by sucrose gradient ultracentrifugation. The  
771 nucleosomes were concentrated, supplemented with 0.02 % NP40 and stored at 4 °C.

## 772 **Optical tweezers assay of Pol II transcription through the nucleosome**

773 Transcription was performed in TB50 buffer. NTPs concentration was 0.5 mM each of ATP, CTP, GTP, UTP.  
774 The 1.5 kb biotins beads were pre-incubated with 0.5  $\mu$ M neutravidin for 10 min at room temperature and  
775 diluted with TB50. Pol II sample beads were prepared by ligating the 1  $\mu$ m 2 kb spacer DNA beads, Pol II  
776 stalled complex, 8  $\times$  repeat DNA and nucleosome loaded on NPS-Xlink (or bare NPS-Xlink DNA) using *E.*  
777 *Coli* DNA ligase (NEB) at 16  $^{\circ}$ C for 2 hours. 0.02% of NP40 was also included in the ligation reaction. The  
778 overhangs of the various components were optimized such that the ligation occurs at desired orders. The  
779 sample beads were diluted with TB50 + 0.02% NP40. The full sequence of the assembled transcription  
780 template was available at the end of the document.

781 To perform the experiment, we first captured a 1.5 kb biotin bead in one trap followed by a Pol II  
782 sample bead in the other trap. The two beads were rubbed against each other until a tether is formed. If the  
783 tether has expected length, the pair of beads was moved to the experimental position, which is close to the  
784 outlet of the NTPs channel. Force feedback was turned on to maintain a constant force of 10 pN and the NTPs  
785 channel was opened to start transcription. Data acquisition was started right after force feedback was turned on  
786 and terminated once the polymerase reached the end or arrested for more than 300 seconds without dynamics.  
787 To probe the fate of transcribed nucleosomes, force feedback was turned off and the trap distance was reset to  
788 a value that gives less than 1 pN force on the tether. The two beads were pulled away from each other by  
789 increasing trap distance at a constant speed of 20 nm/s, until the force reaches above 40 pN. From these pulling  
790 curves, we rarely detected rips normally associated with nucleosome unwrapping. Trap distance was further  
791 increased to break the tether and the beads were calibrated. All transcription data was recorded at 800 Hz.

## 792 ***In vitro* Pol II transcription on the 1 $\times$ repeat template**

793 The 1 $\times$ repeat DNA template was amplified from pGM3z-1 $\times$ repeat plasmid using oligos ZC24-ZC25, digested  
794 with BsaI-HF and purified by agarose gel extraction. To determine the main pause site in the 64 bp repeat  
795 sequence, Pol II stalled complex was radioactively labeled with [ $\alpha$ -<sup>32</sup>P]-ATP during initial pulsing. The stalled  
796 complex was loaded on streptavidin-coated magnetic beads. The beads were washed with TB130 (20mM Tris,  
797 pH=8.0, 130 mM KCl, 5 mM MgCl<sub>2</sub>, 10 mM DTT, 20  $\mu$ g/mL BSA) and ligated to the 1 $\times$ repeat DNA template  
798 using T4 DNA ligase for 1 hour at RT. Transcription was chased by adding 40  $\mu$ M NTPs mix (ATP, UTP,  
799 CTP, GTP, final concentration of 40  $\mu$ M each) to the stalled complex beads, and terminated by adding 2 $\times$  urea  
800 stop buffer (8 M urea, 50 mM EDTA) at 10, 20, 40, 60, 120, 300, 600 and 900 seconds. In parallel,  
801 transcription was chased by adding 40  $\mu$ M NTPs mix together with 50  $\mu$ M of each type of 3'-deoxynucleotide  
802 RNA chain terminators (3'dATP, 3'dCTP, 3'dGTP, 3'dUTP, TriLink Biotechnologies). The reactions were  
803 allowed to proceed at room temperature for 10 min before terminated by adding the 2 $\times$  urea stop buffer.  
804 Samples were extracted with Phenol: Chloroform: Isoamyl alcohol (1:0.9:0.01), precipitated with ethanol and  
805 dissolved in 2 $\times$  formamide sample buffer (95% formamide, 5mM EDTA, pH 8.0, with bromophenol blue and

806 xylene cyanol). RNA was resolved on 12 % denaturing PAGE, dried and exposed to a phosphorimager screen.  
807 Images were captured on the Typhoon imager (GE Healthcare) and processed by ImageJ.

## 808 **Mechanical model for Pol II transcription through the nucleosome**

### 809 *Pol II dynamics*

810 Our model for Pol II dynamics is illustrated in Figure 7B. In this model, Pol II takes forward main pathway  
811 steps by one base pair at a rate  $k_0$  or can enter a backtracked pathway by stepping back one base pair at rate  $k_{b1}$ .  
812 Once backtracked, Pol II takes steps one base pair forward at rate  $k_{fn}$  and steps one base pair backward at rate  
813  $k_{bn}$ . Stepping forward from the first backtracked state returns Pol II to the main pathway.

814 Transition rates depend on force  $f$ , with main pathway and backtracking step rates given by

$$k_0(f) = k_0^0 e^{\delta_0 \ell f / (k_B T)},$$

○ 1 ○

$$k_{fn} = k_{fn}^0 e^{\delta_{fb} \ell f / (k_B T)} \text{ and } k_{bn} = k_{bn}^0 e^{-(1-\delta_{fb}) \ell f / (k_B T)}.$$

817  
818  
819  $k_0^0$ ,  $k_{fn}^0$ , and  $k_{bn}^0$  are the zero force rate constants.  $\delta_0$  and  $\delta_{fb}$  are splitting factors, representing the  
820 transition state location.  $\ell=0.34$  nm is the step size, the length of one DNA base pair.  $k_B T = 4.11$  pN·nm is the  
821 thermal energy at room temperature.

822 Our model is adapted from the Pol II dynamics model and parameterization of Dangkulwanich et al<sup>52</sup>.  
823 Dangkulwanich models Pol II forward stepping as three stages, with the first two reversible, and the third  
824 effectively irreversible. Our experimental condition of high nucleotide concentration leads to a nearly  
825 instantaneous second transition, and we combine the two remaining transitions into a single irreversible  
826 transition with rate  $k_0$ . The zero-force forward rates of the two remaining stages in Dangkulwanich are  $88$  s<sup>-1</sup>  
827 and  $35$  s<sup>-1</sup>, combined into  $k_0^0 = 25$  s<sup>-1</sup>. The rate of initial backstepping,  $k_{b1}$ , is only from the first of the three  
828 main pathway states in Dangkulwanich. Accordingly, we weight this zero-force initial backtracking rate,  $6.9$   
829 s<sup>-1</sup>, by the probability of being in the main pathway state eligible for backtracking,  $k_{b1}^0 = (35/66) \cdot 6.9$  s<sup>-1</sup>.  
830 Backtracking is restricted to a maximum of three base pairs, such that  $k_{bn}=0$  for  $n \geq 4$ . The remaining  
831 parameters are  $k_{fn}^0 = 1.3$  s<sup>-1</sup> for all  $n$ ,  $k_{bn}^0 = 1.3$  s<sup>-1</sup>  $1 \leq n \leq 3$ ,  $\delta_0 = 0.64$ , and  $\delta_{fb} = 0.5$ , taken directly from  
832 Dangkulwanich.

### 833 *Nucleosome effect on polymerase kinetics*

834 The model above describes transitions of the polymerase on DNA, but does not incorporate the effect of the  
835 nucleosome, which is expected to hinder forward stepping. We adapt a previous model<sup>29</sup> to describe the DNA  
836 polymerase-nucleosome system on a two-dimensional energy landscape ( $E_{j,w}$ ). The first dimension ( $j$ ) is the  
837 position of the polymerase and the second ( $w$ ) is the number of DNA base pairs unwrapped from the  
838 nucleosome. This energy landscape incorporates the mechanics of the DNA, polymerase, and nucleosome

839 interaction (namely, steric exclusion between polymerase and nucleosome and bending of the unwrapped DNA)  
840 as described in the section below.

841 For a given length of unwrapped DNA, there is a change in energy associated with the polymerase  
842 stepping forward,

$$\Delta E_{j,w} = E_{j+1,w} - E_{j,w},$$

844 which modulates the rate of that step according to  
845

$$846 \quad k_0^{(j,w)}(f) = k_0^0 \exp[\delta_0(\ell f - \Delta E_{j,w})/(k_B T)].$$

847  
848 This assumes that the step forward involves a transition state at fractional position  $\delta_0$  and that the  
849 energy landscape is linear between positions  $j$  and  $j+1$ .

850 We assume that the wrapping and unwrapping of DNA from the nucleosome is much faster than the  
851 polymerase stepping kinetics. In this case, the system is equilibrated along the  $w$  dimension, and the overall  
852 stepping rate for the polymerase can be described as a weighted average over all the stepping rates:

$$k_0^{(j,\text{eff})} = \left( k_0^0 e^{\frac{\delta_0 \ell f}{k_B T}} \right) \frac{\sum_w e^{-E_{j,w}} e^{-\delta_0 \Delta E_{j,w}}}{\sum_w e^{-E_{j,w}}}$$

855

856  
857 An analogous calculation is done for the forward and backward stepping rates in the backtracked state:

$$k_{bn}^{(j,\text{eff})} = \left( k_{bn}^0 e^{\frac{(1-\delta_{fb})\ell f}{k_B T}} \right) \frac{\sum_w e^{-E_{j,w}} e^{(1-\delta_{fb})\Delta E_{j-1,w}}}{\sum_w e^{-E_{j,w}}}$$

$$k_{fn}^{(j,\text{eff})} = \left( k_{fn}^0 e^{\frac{\delta_{fb}\ell f}{k_B T}} \right) \frac{\sum_w e^{-E_{j,w}} e^{-\delta_{fb}\Delta E_{j,w}}}{\sum_w e^{-E_{j,w}}}$$

862

863  
864  
865 (all the energies in the above are expressed in units of  $k_B T$ ). Overall, the presence of the nucleosome  
866 modifies the polymerase kinetics by making it much slower to step forward if doing so would require a  
867 substantial increase in energy associated with bending of the linker DNA ahead of the polymerase.

### 868 *Energy landscape for polymerase–nucleosome system*

869 The free energy  $E_{jw}$  is defined by the location of the polymerase at basepair  $j$  (relative to the start of the  
870 nucleosome) and the number of DNA base pairs unwrapped from the nucleosome,  $w$ .

$$871 \quad E_{jw} = E_N^{(L)} + E_{\text{int}}.$$

872

873 The first term  $E_N^{(L)}$  is the conformation energy for the DNA linker  $N$  base pairs in length between Pol  
874 II and the nucleosome<sup>29</sup>. We use a highly simplified mechanical model for this system, where the histone core  
875 of the nucleosome is treated as a steric sphere of radius  $R_{\text{nuc}}=3.2\text{nm}$  and Pol II is treated as a steric sphere of  
876 radius  $R_{\text{pol}}=7\text{ nm}$ . The DNA is modeled as a wormlike chain with  $35.4\text{nm}$  persistence length, that must stretch  
877 from the center of the polymerase to positions along a spiral wrapped around the nucleosome (Figure 7A). For  
878 a given length of DNA unwrapped ahead of the polymerase ( $\ell N$ ), the bending energy is calculated by  
879 optimizing the wormlike chain configuration subject to the constraint that the steric spheres for polymerase and  
880 nucleosome may not overlap. If very little DNA is unwrapped ahead of the polymerase, the linker is short and  
881 must bend tightly to avoid steric overlap (leading to high energies). If more of the DNA is unwrapped, the  
882 linker may not need to bend at all ( $E_N^{(L)} = 0$  for lengths above approximately 30 bp).

883 The second contribution  $E_{\text{int}}$  is the energy of DNA interaction with the nucleosome. This includes  
884 unfavorable bending of the DNA around the nucleosome and favorable DNA-nucleosome binding interactions.  
885  $N_{\text{tot}}=147$  base pairs can bind to the nucleosome, and each can have a different interaction energy. For  $w$  DNA  
886 base pairs unwrapped from the nucleosome

$$E_{\text{int}} = \sum_{i=w+1}^{N_{\text{tot}}} \phi_i ,$$

887  
888  
889  
890  
891 where  $\phi_i$  is the interaction energy of  $i$ 'th base pair with the nucleosome.

## 892 ***Determining dwell times and fitting***

893 With the quantitative model of polymerase dynamics, we can determine mean dwell times. We analytically  
894 determine the mean time for the polymerase to reach the  $n+1$ 'th state after first reaching the  $n$ 'th state<sup>29</sup>.

895 This model assumes the binding/unbinding of the DNA ahead of the polymerase is always  
896 equilibrated as the polymerase steps backward and forward. This is a reasonable assumption, given the rapid  
897 equilibration time for DNA unwrapping, but only up to the point when the DNA fully unwraps from the  
898 nucleosome. Our model neglects the additional entropic contributions of DNA and polymerase separating  
899 completely in solution and cannot properly predict the dwell times at the very end of the polymerase  
900 transcribing through the nucleosome.

901 Using the lsqcurvefit routine in Matlab, we fit the DNA-nucleosome interaction energies  $\phi_i$  to match  
902 the quantitative model mean dwell times to the experimental mean dwell times, smoothed by taking the local  
903 average over a 3-bp span. As shown in Figure 7D, we only include experimental mean dwell time where the  
904 polymerase is positioned within the nucleosomal binding sequence ( $j \geq 0$ ). Prior to these base pairs, we use a  
905 mean dwell time  $(k_0^0)^{-1} = 0.04\text{ s}$ .

## 906 Data Analysis

### 907 *Single-molecule unzipping data analysis*

908 Using the calibration data, we calculated the complete force-extension curves for each tether. The analysis  
909 consisted of the following steps:

910 First, the relaxation of the fully unzipped construct (that is, after the complete unzipping of the  
911 construct and before re-zipping of dsDNA has begun, corresponding to a force range of ~ 20-40 pN) was fit to a  
912 model in which 1850 bp of dsDNA are described as a worm-like chain with a persistence length of 35.4 nm, a  
913 stretch modulus of 1020 pN and a contour of 0.34 nm/bp<sup>53,54</sup>, and 872 bases of ssDNA are described using an  
914 extensible freely jointed chain with a contour length of 0.59 nm/base<sup>55,56</sup>. The dsDNA parameters were  
915 estimated by analyzing the pulling curves of 4.7 kb dsDNA molecules. The other parameters (stretch modulus  
916 and Kuhn lengths for the ssDNA and an offset of the extension to account for bead size variation) were fit,  
917 resulting in a Kuhn length of  $1.45 \pm 0.02$  nm, a stretch modulus of  $975 \pm 61$  pN and an offset of  $29 \pm 2$  nm  
918 (errors are 95% confidence intervals over all traces,  $N = 234$ ). These values are close to previously published  
919 values<sup>57</sup>. Using these parameters we calculated the number of unzipped base pairs at all positions along the  
920 pulling trace.

921 Second, we performed a minor adjustment on the extension to align the two NPS repeats on the bare  
922 DNA template. In principle, identical positions in the two NPS repeats should be 197 bp apart in distance, and  
923 they are expected to behave identically in the trace (same force-extension signatures). However, the calculated  
924 distance obtained initially is typically different from this value of 197 bp. At this point, we rescaled the data  
925 along the x-axis (number of unzipped base pairs) to maintain 436 unzipped base pairs at the end of the  
926 unzipping curve and a distance of 197 base pairs between identical positions on the two NPS sequences. To  
927 find the correct scaling factor, we rescaled the data using a range of scaling factors (from 170-197) using the  
928 following equation:

929

$$N_{rescaled} = 436 - \frac{197}{factor} \times (436 - N_{not\_rescaled})$$

930

931 For each factor, we binned the data points in 0.5 bp window and calculated the force-weighted  
932 residence histogram along the sequence. We then calculated the correlation between the histogram at positions  
933 along the first NPS and the histogram at positions along the second NPS:

934

$$Correlation = \sum_{first\_copy\_i} Res(first\_copy\_i) \times Res(first\_copy\_i + 197)$$

935

936 The factor giving the maximum correlation was selected, and the data was finally rescaled using this  
937 factor. Using this approach, we generated a mean residence histogram of the first NPS from all bare DNA  
938 unzipping traces. The rescaling factors were typically between 180 to 190. The requirement for rescaling to  
939 satisfy the periodicity may result from bead size variations or deviations from the models used to describe the  
940 pulling traces.

941 Third, once an aligned mean residence histogram of the first NPS was obtained from unzipping traces  
942 of bare DNA, a slightly modified operation was performed on unzipping traces of the nucleosome datasets.  
943 Again, the relaxation after complete unzipping was fit and the number of unzipped base pairs were calculated,  
944 and again rescaled using a range of rescaling factors. This time, the correlation between the residence time  
945 histogram of the first NPS in the nucleosome traces and the mean residence histogram of the first NPS  
946 obtained in the previous step was calculated and maximized. The rescaling factors for nucleosome data had the  
947 same range as for the bare DNA data.

#### 948 ***Residence time analysis of unzipping traces***

949 After obtaining the fitting parameters for both dsDNA and ssDNA, bead-to-bead distances of the unzipping  
950 traces were converted to unzipped basepairs. The unzipped basepairs of the traces were then aligned, scaled  
951 and normalized to the beginning of the second NPS by subtracting 248 bp (the second NPS begins at 249 bp of  
952 the Y stem region). For traces obtained at constant trap separation speed (20 nm/s), a force weighted residence  
953 time (RT) between each bp was calculated by summing the forces of all data points between two consecutive  
954 unzipped basepairs (Figure 1E). Therefore, long residence time (i.e. more data points) while under higher force  
955 within a particular bp would result in a high force-weighted RT in this analysis. The force weighted RT  
956 accounts for force differences along the unzipping trace and serves as a proxy of the strength of histone-DNA  
957 interactions of the nucleosome. For constant force unzipping traces, residence time at each bp was calculated  
958 by counting intervening data points  $N$ . Because data frequency is 800 Hz, RT therefore equals to  $N/800$   
959 (Figure 2C). RT histograms are plotted as mean values from all traces.

#### 960 ***Analysis of the number of unzipping transitions in unzipping traces***

961 A transition in the unzipping trace is defined as a peak in the residence time histogram that is above a certain  
962 threshold. For each unzipping trace obtained at constant trap separation speed, we identified transition events  
963 by looking for maxima in the RT histogram and manually applying a threshold to avoid too many transitions  
964 (rips) from just bare DNA. The chosen threshold cannot be too high, as the RT for H2A.Z unzipping traces  
965 generally have more peaks but lower amplitude for each peak. This analysis (Figure S1F) revealed that on  
966 average, H2A.Z nucleosome unzipping traces have at least one more ripping transition than those of WT  
967 nucleosomes.

968 *Analysis of the partial unzipping data to test mobility*

969 The final unzipping trace or the bare DNA unzipping trace was used to fit the WLC model to obtain the  
970 elasticity, offset and scaling parameters of a particular tether. These parameters are applied to previous partial  
971 unzips from the same tether. All traces for a particular tether are plotted together without any further  
972 alignments. Note, for both WT and H2A.Z nucleosomes, the initial force rise always occurs at the same  
973 position without lateral shifts. During the force rise at the proximal dimer region, the unzipping fork randomly  
974 dwells at nearby locations ( $\sim 5$  bp away), consistent with nucleosome hopping in this region.

975 *Analysis of hopping (equilibrium) data at constant trap positions*

976 To explore steady-state behavior of DNA on the nucleosome, the trap separation was held fixed such that the  
977 DNA experiences wrapping and unwrapping fluctuations in the proximal dimer region, ‘hopping’ on and off  
978 the nucleosome. A trace of force-extension pairs is measured at each trap separation (Figure S3F), followed by  
979 a final unzipping and relaxation trace at constant trap velocity. The following subsections describe our analysis  
980 methods for extracting from this data an underlying energy landscape for DNA base pairing energies and the  
981 energies of interaction with the nucleosome.

982 *Calculation of unzipping energies from force-extension traces*

983 Because the pulling and extension curves for bare DNA overlap closely with no hysteresis (Figure 1B), we  
984 assume this process is at equilibrium. The energy associated with unzipping each basepair can then be  
985 computed from the work done by the pulling force during unzipping, with a correction for the work required to  
986 extend the newly unzipped bases.

987 To start, we find the fractional extension of dsDNA worm-like chains and ssDNA freely jointed  
988 chains at a given force,  $z_{ds}(F)$  and  $z_{ss}(F)$ , respectively<sup>58</sup>. The length of ssDNA  $L_{ss}$  between the two dsDNA  
989 handles of length  $L_{ds}$  for each force-extension pair ( $F, s$ ) is then given by

$$L_{ss} = \frac{s - 2z_{ds}(F)L_{ds}}{z_{ss}(F)}$$

992

993 The number of base pairs unzipped is

$$N_{\text{unzip}} = \frac{L_{ss}}{2\ell_{ss}},$$

996

997 where  $\ell_{ss}$  is the ssDNA length per base pair, with a factor of two because twice the base pair length of  
998 ssDNA is obtained when unzipping one base pair of dsDNA. Each number of base pairs unzipped  $N_{\text{unzip}}$  can  
999 now correspond to a specific force  $F$ , length of ssDNA  $L_{ss}$ , and fractional extension of ssDNA  $z_{ss}$ . The  
1000 unzipping energy of each base pair of ssDNA is the overall work to extend the two newly unzipped bases  
1001 minus the work required to stretch those bases to the observed extension.



1002

$$\Delta E_{\text{unzip}}(N_{\text{unzip}}) = 2Fz_{\text{ss}}\ell_{\text{ss}} - \int_0^{2\ell_{\text{ss}}z_{\text{ss}}} F_{\text{FJC}}(x)dx .$$

1003 ***Alignment of force-extension data***

1004 Because the bead radius cannot be known precisely, individual data collection runs are shifted arbitrarily along  
1005 the extension axis. We use the final complete pulling curve to account for this shift. The pulling curves for  
1006 each experimental run with bare DNA are first mutually aligned (Figure S3C) and the average trace is used to  
1007 calculate the absolute shift along the extension axis.

1008 Specifically, we calculate the unzipping energy for each basepair as described in the previous section.  
1009 The two copies of the NPS give rise to duplicate features in the base-pair interaction energy landscape, whose  
1010 separation depends on the absolute values of the end-to-end extension input into the calculation. We therefore  
1011 shift the averaged force-extension curve along the x axis in such a way that the duplicate energy features are  
1012 separated by precisely 197 bp (Figure S3D). The same shift is assumed for the equilibrated hopping data  
1013 obtained for each individual DNA molecule prior to the corresponding pulling trace. No scaling of the x-axis is  
1014 done in this analysis.

1015 In our calculations we used dsDNA persistence length of 35.4 nm, dsDNA stretching modulus 1020  
1016 pN, 0.34 nm contour length per base pair, ssDNA segment length 1.03 nm, ssDNA stretching modulus 1000  
1017 pN, 0.59 nm contour length per base pair. The ssDNA parameters were obtained by fitting the final region of  
1018 the averaged pulling curve for bare DNA traces, where the hairpin has been completely unzipped. The  
1019 calculated force-extension relation for a molecule with a 434 bp unzippable region, terminated with a 4-base  
1020 hairpin, and connected to two dsDNA handles (1848 bp), given the fitted unzipping energies, is shown in  
1021 Figure S3E.

1022 Pulling traces with bound nucleosomes present are aligned to the averaged pulling trace for bare DNA  
1023 based on the force-extension curve features prior to reaching the second NPS (specifically, extensions below  
1024 870 nm are used for alignment).

1025 ***Extracting DNA-nucleosome interaction energies from equilibrated hopping data***

1026 For each trap separation, the number of base pairs unzipped ( $N$ ) is obtained for each force-extension pair,  
1027 populating a distribution in  $N$  (Figure 3B). Assuming the system is in thermodynamic equilibrium, the  
1028 probability for each number of base pairs unzipped is converted to a relative energy for each number of base  
1029 pairs unzipped. Subtracting the energy of DNA stretching and the energy for the off-center beads in the optical  
1030 traps gives the cumulative relative energy to unzip the given number of base pairs. The difference in this  
1031 cumulative relative energy between consecutive base pairs is the energy to unzip each base pair. The various  
1032 fixed trap separations provide overlapping ranges for the energy of unzipping for each basepair (Figure S3G),  
1033 and the average value from all trap separations that span a particular value of  $N$  is used for further analysis.

1034 To find the energy of the DNA-nucleosome interactions, the unzipping energy for bare DNA (no  
1035 nucleosome present) is subtracted from the unzipping energy for a system with a nucleosome present (WT,  
1036 H2A.Z, and uH2B).

1037 Given the extracted energies of unzipping bare DNA and peeling DNA off the nucleosome for the  
1038 region accessed by the equilibrium hopping data, we can calculate the predicted force extension relation in an  
1039 equilibrium pulling curve (Figure S3H). We note that the observed forces in the nucleosome-bound region  
1040 during the constant velocity pulling traces are substantially higher, emphasizing that these traces are obtained  
1041 out of equilibrium.

#### 1042 *Nucleosome transcription data analysis*

1043 The alignment of the “molecular ruler”, data analysis on pausing, backtracking and residence time of Pol II  
1044 was performed essentially the same as recently described<sup>22</sup>. Briefly, for each trace the region expected to  
1045 contain the repeats ( $8 \times 64$  bp) was aligned to find the physical length of the repeat in nanometers, and the  
1046 aligned traces were aligned between themselves and to the known pause sites discovered by biochemical  
1047 studies (described below). The pause site within each repeat is located at the 59<sup>th</sup> nucleotide (T) of the 64 bp  
1048 DNA and the periodicity of the physical length of each repeat is found to be 21.1 nm at 10pN force. The  
1049 position of the polymerase along the nucleosome was obtained by extrapolating the position from the aligned  
1050 repeat region. To plot the transcribed distance (bp) of the leading edge of Pol II relative to NPS, we applied an  
1051 offset of 16 bp to account for the footprint of Pol II.

1052 The crossing time is calculated as the total duration of the leading edge of Pol II crossing the entire  
1053 147 bp NPS region. Only traces that reached the stall site are included in crossing time analysis.

1054 Example traces of Pol II hopping at certain regions (Figure S5) were analyzed with a classic Hidden  
1055 Markov Model (HMM) by fitting to two (for hWT or H2A.Z) or three states ( for uH2B).

1056 Probability of arresting is calculated as the percentage of traces that entered NPS but did not reach the  
1057 stall site, while probability of crossing is the percentage of traces that successfully reached the stall site.  
1058 Typically, we considered a trace that paused 300s or longer without any associated dynamics to be arrested.  
1059 For arrested traces, percentages of traces that arrested before or after the dyad are also calculated based on their  
1060 arrest position.

1061 Pause-free velocities (bp/s) of Pol II before, inside and after NPS are estimated by calculating the  
1062 inverse of the median residence time (s/bp) at distinct sites. To account for sequence bias, the three fastest sites  
1063 (lowest median residence time) are chosen from each sampling range. For regions before or after NPS, sites  
1064 up to 100 bp away from the NPS region are sampled.

#### 1065 **Full sequence of the unzipping template**

1066 The sequence below shows the stem of the Y structure that contains two consecutive pieces of NPS DNA  
1067 (green and yellow). The red sequence is the stem of the end hairpin (four bases of the loop not shown here).

1068 The 147 bp core '601' NPS is underlined in each segment. The upstream DNA is bridged to the two arms of  
1069 the Y. The DNA in between are ligation sites. The full length of ssDNA after complete unzipping will be 872  
1070 bases (including extra bases from the loop of the hairpin).

1071 (arms)...TTTGGACTACTGACGCGGACATTCAGGA GATGGACCCTATACGCGGCCGCCCTGGAGAA  
1072 TCCCGGTGCCGAGGCCGCTCAATTGGTCGTAGACAGCTCTAGCACCGCTTAAACGCACGTACGCC  
1073 CTGTCCCCCGCGTTTTAACCGCCAAGGGGATTACTCCCTAGTCTCCAGGCACGTGTCAGATATA  
1074 ACATCCTGTGCATGTATTGAACAGCGACCTTGCAAC GATGGACCCTATACGCGGCCGCCCTGGAG  
1075 AATCCCGGTGCCGAGGCCGCTCAATTGGTCGTAGACAGCTCTAGCACCGCTTAAACGCACGTACG  
1076 CGCTGTCCCCCGCGTTTTAACCGCCAAGGGGATTACTCCCTAGTCTCCAGGCACGTGTCAGATAT  
1077 ATACATCCTGTGCATGTATTGAACAGCGACCTTGCACCCT **CCACTCTAGA**

### 1078 Full sequence of the Pol II transcription template

1079 Pol II loading sequence (NDS/TDS), 8 × repeat DNA, core '601' NPS and crosslinked DNA (Xlink) are  
1080 highlighted in cyan, green, yellow and red, respectively. The transcription starvation site (T in NDS) is bolded  
1081 and underlined. The NPS-Xlink DNA used for octamer loading is underlined.

1082 AGGTCTCAGAAGACGCCCGAACAACAGACACAAACACCACGGCCGGCGAGCCAGACACGACCA  
1083 ATTATCTATGTAACCTGCCATATTCAGGATTATCAGTAGCGGAAGAGCGAGCTCGGTACCCGATC  
1084 CAGATCCCGAACGCCTATCTTAAAGTTTAAACATAAAGACCAGACCTAAAGACCAGACCTAAAG  
1085 ACACTACATAAAGACCAGACCTAAAGACGCCTTGTTGTTAGCCATAAAGTGATAACCTTTAATCA  
1086 TTGTCTTTATTAATACTACTATAAGAAGAGACAACCTTAAAGAGACTTAAAAGATTAATTTA  
1087 AAATTTATCAAAAAGAGTATTGACTTAAAGTCTAACCTATAGGATACTTACAGCCATCGAGAGGG  
1088 ACACGGGGAAACACCACCAGCCT CCCGGGCTCACCATCATCCTGACTAGTCTTTCAGGCGATGTG  
1089 TGCTGGAAAGATCTTATGTCACCCCGGGCTCACCATCATCCTGACTAGTCTTTCAGGCGATGTGTG  
1090 CTGGAAAGATCTTATGTCACCCCGGGCTCACCATCATCCTGACTAGTCTTTCAGGCGATGTGTGCT  
1091 GGAAAGATCTTATGTCACCCCGGGCTCACCATCATCCTGACTAGTCTTTCAGGCGATGTGTGCTG  
1092 GAAAGATCTTATGTCACCCCGGGCTCACCATCATCCTGACTAGTCTTTCAGGCGATGTGTGCTGG  
1093 AAAGATCTTATGTCACCCCGGGCTCACCATCATCCTGACTAGTCTTTCAGGCGATGTGTGCTGGA  
1094 AAGATCTTATGTCACCCCGGGCTCACCATCATCCTGACTAGTCTTTCAGGCGATGTGTGCTGGAA  
1095 AGATCTTATGTCACCCCGGGCTCACCATCATCCTGACTAGTCTTTCAGGCGATGTGTGCTGGAAA  
1096 GATCTTATGTCACCCCGTGGATCCGCCGGCCGCAACGATGGACCCTATACGCGGCCGCC CTGGAG  
1097 AATCCCGGTGCCGAGGCCGCTCAATTGGTCGTAGACAGCTCTAGCACCGCTTAAACGCACGTACG  
1098 CGCTGTCCCCCGCGTTTTAACCGCCAAGGGGATTACTCCCTAGTCTCCAGGCACGTGTCAGATAT  
1099 ATACATCCTGTGCATGTATTGAACAGCGACCTTGCCGGTGCCAGTCGGATAGTGTTCGAGCTCC  
1100 CACTCTAGAGGATCCCGGGTACCGAGCTCGAATTCGCCCTATAGTGAGTCGTATTACAATTCAC  
1101 TGGCCGTCGCACCCT **GGTGTACAGAACGCAATGAATT**

1102 **Full sequence of the 1 × repeat template for *in vitro* transcription**

1103 The 1× 64 bp repeat sequence is highlighted in green.

1104 CAACGCCT **CCC GGG CTC ACC ATC AT CCT GACT AGT CTT TCAGG CGAT GTGTGCTGGAAAGATCTT**  
1105 **ATGTCAC** CCCGTGGATCCGCCGGCCGTCATCACCATCATCCTGACTAGAGTCCTTGCCGAACCGG  
1106 TGT TTGACGTCCAGGAATGTCAAATCCGTGGCGTGACCTATCCGCACCGCTGCG

1107 **Movies**

1108 Movie-M1: Unzipping-rezipping of bare NPS DNA

1109 Movie-M2: Unzipping-rezipping of hWT nucleosome

1110 Movie-M3.1: Pol II transcription through bare NPS DNA

1111 *(the horizontal grey dashed lines indicate predicted pause sites in the molecular ruler, the three horizontal*  
1112 *black dashed lines represent NPS entry, dyad, and NPS exit, respectively. This applies to all other movies)*

1113 Movie-M3.2: Pol II transcription through bare NPS DNA, NPS zoom

1114 Movie-M4.1: Pol II transcription through xWT nucleosome

1115 Movie-M4.2: Pol II transcription through xWT nucleosome, NPS zoom

1116 Movie-M5.1: Pol II transcription through hWT nucleosome

1117 Movie-M5.2: Pol II transcription through hWT nucleosome, NPS zoom

1118 Movie-M6.1: Pol II transcription through H2A.Z nucleosome

1119 Movie-M6.2: Pol II transcription through H2A.Z nucleosome, NPS zoom

1120 Movie-M7.1: Pol II transcription through uH2B nucleosome

1121 Movie-M7.2: Pol II transcription through uH2B nucleosome, NPS zoom

1122

1123 **Data and code availability**

1124 Raw data will be made available via Dryad [DOI here]

1125 Matlab scripts have been deposited in github at <https://github.com/lenafabr/dataprocessDNAunzipping>

1126

1127 **Acknowledgements**

1128 We thank Prof. Craig D. Kaplan (University of Pittsburgh) for providing us biotinylated yeast  
1129 Pol II, Guillermo Chacaltana and Robert Sosa for technical assistance, and all members of  
1130 Bustamante laboratory for critical discussion. This work was supported by Howard Hughes  
1131 Medical Institute, NIH Grants R01GM032543 and R01GM071552 to C.B., R01GM098401 to  
1132 T.Y., the US Department of Energy Office of Basic Energy Sciences Nanomachine Program  
1133 under Contract DE-AC02-05CH11231 to C.B., a grant from Alfred P. Sloan Foundation to E.F.K.

1134 (FG-2018-10394), and a Burroughs Wellcome Fund Collaborative Research Travel Grant to T.Y.;  
1135 C.B. is a Howard Hughes Medical Institute Investigator.

1136

## 1137 **Author Contributions**

1138 Z.C., R.G., T.Y., and C.B. conceived the study. Z.C., R.G., and T.Y. designed nucleosome  
1139 unzipping experiments. Z.C. and R.G. designed Pol II transcription experiments. Z.C. performed  
1140 the single molecule experiments and collected data with assistance from R.G. and T.Y.. Z.C.,  
1141 R.G., and A.L. developed the ‘molecular ruler’. Z.C., A.L., R.G., A.B., and E.K. analyzed  
1142 nucleosome unzipping and hopping data. Z.C., R.G., A.L., A.B., and E.K. analyzed Pol II  
1143 transcription data. A.B. and E.K. developed the mechanical model. Z.C., A.S., and T.Y.  
1144 assembled all human nucleosomes. C.D. assembled *Xenopus* nucleosome. C.K. provided  
1145 biotinylated yeast Pol II. Z.C. wrote the initial draft of the manuscript. Z.C., A.B., E.K., T.Y.,  
1146 and C.B. edited the manuscript. All authors discussed the results and commented on the  
1147 manuscript. T.Y. and C.B. supervised the study.

1148

## 1149 **Declaration of Interests**

1150 The authors declare no competing interests.

1151

## 1152 **REFERENCES**

- 1153 1. Bondarenko, V. A. *et al.* Nucleosomes can form a polar barrier to transcript elongation by  
1154 RNA polymerase II. *Mol. Cell* **24**, 469–79 (2006).
- 1155 2. Hall, M. A. *et al.* High-resolution dynamic mapping of histone-DNA interactions in a  
1156 nucleosome. *Nat. Struct. Mol. Biol.* **16**, 124–129 (2009).
- 1157 3. Ngo, T. T. M., Zhang, Q., Zhou, R., Yodh, J. G. & Ha, T. Asymmetric unwrapping of  
1158 nucleosomes under tension directed by DNA local flexibility. *Cell* **160**, 1135–44 (2015).
- 1159 4. Weber, C. M., Ramachandran, S. & Henikoff, S. Nucleosomes are context-specific,  
1160 H2A.Z-modulated barriers to RNA polymerase. *Mol. Cell* **53**, 819–30 (2014).
- 1161 5. Rhee, H. S., Bataille, A. R., Zhang, L. & Pugh, B. F. Subnucleosomal Structures and  
1162 Nucleosome Asymmetry across a Genome. *Cell* **159**, 1377–1388 (2014).
- 1163 6. Teves, S. S., Weber, C. M. & Henikoff, S. Transcribing through the nucleosome. *Trends*

- 1164 *Biochem. Sci.* **39**, 577–86 (2014).
- 1165 7. Hodges, C., Bintu, L., Lubkowska, L., Kashlev, M. & Bustamante, C. Nucleosomal  
1166 fluctuations govern the transcription dynamics of RNA polymerase II. *Science* **325**, 626–8  
1167 (2009).
- 1168 8. Bintu, L. *et al.* Nucleosomal elements that control the topography of the barrier to  
1169 transcription. *Cell* **151**, 738–749 (2012).
- 1170 9. Mihardja, S., Spakowitz, A. J., Zhang, Y. & Bustamante, C. Effect of force on  
1171 mononucleosomal dynamics. *Proc. Natl. Acad. Sci. U. S. A.* **103**, 15871–6 (2006).
- 1172 10. Righini, M. *et al.* Full molecular trajectories of RNA polymerase at single base-pair  
1173 resolution. *Proc. Natl. Acad. Sci. U. S. A.* **115**, 1286–1291 (2018).
- 1174 11. Fitz, V. *et al.* Nucleosomal arrangement affects single-molecule transcription dynamics.  
1175 *Proc. Natl. Acad. Sci. U. S. A.* **113**, 12733–12738 (2016).
- 1176 12. Rudnizky, S. *et al.* H2A.Z controls the stability and mobility of nucleosomes to regulate  
1177 expression of the LH genes. *Nat. Commun.* **7**, 12958 (2016).
- 1178 13. Lowary, P. . & Widom, J. New DNA sequence rules for high affinity binding to histone  
1179 octamer and sequence-directed nucleosome positioning. *J. Mol. Biol.* **276**, 19–42 (1998).
- 1180 14. Luger, K., Mäder, A. W., Richmond, R. K., Sargent, D. F. & Richmond, T. J. Crystal  
1181 structure of the nucleosome core particle at 2.8 Å resolution. *Nature* **389**, 251–260 (1997).
- 1182 15. Ramachandran, S. & Henikoff, S. Replicating nucleosomes. *Sci. Adv.* **1**, e1500587 (2015).
- 1183 16. Ramachandran, S., Ahmad, K. & Henikoff, S. Transcription and Remodeling Produce  
1184 Asymmetrically Unwrapped Nucleosomal Intermediates. *Mol. Cell* **68**, 1038–1053.e4  
1185 (2017).
- 1186 17. Kireeva, M. L. *et al.* Nucleosome Remodeling Induced by RNA Polymerase II: Loss of  
1187 the H2A/H2B Dimer during Transcription. *Mol. Cell* **9**, 541–552 (2002).
- 1188 18. Ransom, M., Dennehey, B. K. & Tyler, J. K. Chaperoning histones during DNA  
1189 replication and repair. *Cell* **140**, 183–95 (2010).
- 1190 19. Sheinin, M. Y., Li, M., Soltani, M., Luger, K. & Wang, M. D. Torque modulates  
1191 nucleosome stability and facilitates H2A/H2B dimer loss. *Nat. Commun.* **4**, 2579 (2013).
- 1192 20. Clarkson, M. J., Wells, J. R. E., Gibson, F., Saint, R. & Tremethick, D. J. Regions of  
1193 variant histone His2AvD required for *Drosophila* development. *Nature* **399**, 694–697  
1194 (1999).

- 1195 21. Zlatanova, J. & Thakar, A. H2A.Z: View from the Top. *Structure* **16**, 166–179 (2008).
- 1196 22. Gabizon, R., Lee, A., Vahedian-Movahed, H., Ebright, R. H. & Bustamante, C. J. Pause  
1197 sequences facilitate entry into long-lived paused states by reducing RNA polymerase  
1198 transcription rates. *Nat. Commun.* **9**, 2930 (2018).
- 1199 23. Herbert, K. M. *et al.* Sequence-Resolved Detection of Pausing by Single RNA Polymerase  
1200 Molecules. *Cell* **125**, 1083–1094 (2006).
- 1201 24. Landry, M. P., McCall, P. M., Qi, Z. & Chemla, Y. R. Characterization of Photoactivated  
1202 Singlet Oxygen Damage in Single-Molecule Optical Trap Experiments. *Biophys. J.* **97**,  
1203 2128–2136 (2009).
- 1204 25. Shao, W. & Zeitlinger, J. Paused RNA polymerase II inhibits new transcriptional initiation.  
1205 *Nat. Genet.* **49**, 1045–1051 (2017).
- 1206 26. Hsieh, F.-K. *et al.* Histone chaperone FACT action during transcription through chromatin  
1207 by RNA polymerase II. *Proc. Natl. Acad. Sci. U. S. A.* **110**, 7654–9 (2013).
- 1208 27. Batta, K., Zhang, Z., Yen, K., Goffman, D. B. & Pugh, B. F. Genome-wide function of  
1209 H2B ubiquitylation in promoter and genic regions. *Genes Dev.* **25**, 2254–65 (2011).
- 1210 28. Chandrasekharan, M. B., Huang, F. & Sun, Z.-W. Ubiquitination of histone H2B regulates  
1211 chromatin dynamics by enhancing nucleosome stability. *Proc. Natl. Acad. Sci. U. S. A.*  
1212 **106**, 16686–91 (2009).
- 1213 29. Koslover, E. F. & Spakowitz, A. J. Force fluctuations impact kinetics of biomolecular  
1214 systems. *Phys. Rev. E* **86**, 011906 (2012).
- 1215 30. Dangkulwanich, M. *et al.* Complete dissection of transcription elongation reveals slow  
1216 translocation of RNA polymerase II in a linear ratchet mechanism. *Elife* **2**, (2013).
- 1217 31. Farnung, L., Vos, S. M. & Cramer, P. Structure of transcribing RNA polymerase II-  
1218 nucleosome complex. *Nat. Commun.* **9**, 5432 (2018).
- 1219 32. Kujirai, T. *et al.* Structural basis of the nucleosome transition during RNA polymerase II  
1220 passage. *Science (80-. )*. **362**, 595–598 (2018).
- 1221 33. Ehara, H. *et al.* Structural insight into nucleosome transcription by RNA polymerase II  
1222 with elongation factors. *Science (80-. )*. **363**, 744–747 (2019).
- 1223 34. Chen, Y. *et al.* Revealing transient structures of nucleosomes as DNA unwinds. *Nucleic*  
1224 *Acids Res.* **42**, 8767–8776 (2014).
- 1225 35. Bilokapic, S., Strauss, M. & Halic, M. Histone octamer rearranges to adapt to DNA

- 1226 unwrapping. *Nat. Struct. Mol. Biol.* **25**, 101–108 (2018).
- 1227 36. Belotserkovskaya, R. *et al.* FACT Facilitates Transcription-Dependent Nucleosome  
1228 Alteration. *Science (80-. )*. **301**, 1090–1093 (2003).
- 1229 37. Mason, P. B. & Struhl, K. The FACT complex travels with elongating RNA polymerase II  
1230 and is important for the fidelity of transcriptional initiation in vivo. *Mol. Cell. Biol.* **23**,  
1231 8323–33 (2003).
- 1232 38. Chen, P. *et al.* Functions of FACT in Breaking the Nucleosome and Maintaining Its  
1233 Integrity at the Single-Nucleosome Level. *Mol. Cell* **71**, 284–293.e4 (2018).
- 1234 39. Bonisch, C. & Hake, S. B. Histone H2A variants in nucleosomes and chromatin: more or  
1235 less stable? *Nucleic Acids Res.* **40**, 10719–10741 (2012).
- 1236 40. Park, Y.-J., Dyer, P. N., Tremethick, D. J. & Luger, K. A new fluorescence resonance  
1237 energy transfer approach demonstrates that the histone variant H2AZ stabilizes the histone  
1238 octamer within the nucleosome. *J. Biol. Chem.* **279**, 24274–82 (2004).
- 1239 41. Santisteban, M. S., Hang, M. & Smith, M. M. Histone variant H2A.Z and RNA  
1240 polymerase II transcription elongation. *Mol. Cell. Biol.* **31**, 1848–60 (2011).
- 1241 42. Wyce, A. *et al.* H2B ubiquitylation acts as a barrier to Ctk1 nucleosomal recruitment prior  
1242 to removal by Ubp8 within a SAGA-related complex. *Mol. Cell* **27**, 275–88 (2007).
- 1243 43. Zhang, H., Roberts, D. N. & Cairns, B. R. Genome-wide dynamics of Htz1, a histone  
1244 H2A variant that poises repressed/basal promoters for activation through histone loss. *Cell*  
1245 **123**, 219–31 (2005).
- 1246 44. Dyer, P. N. *et al.* Reconstitution of Nucleosome Core Particles from Recombinant  
1247 Histones and DNA. in 23–44 (2003). doi:10.1016/S0076-6879(03)75002-2
- 1248 45. Long, L., Furgason, M. & Yao, T. Generation of nonhydrolyzable ubiquitin–histone  
1249 mimics. *Methods* **70**, 134–138 (2014).
- 1250 46. Whitley, K. D., Comstock, M. J. & Chemla, Y. R. High-Resolution “Fleazers”: Dual-Trap  
1251 Optical Tweezers Combined with Single-Molecule Fluorescence Detection. in *Methods in*  
1252 *molecular biology (Clifton, N.J.)* **1486**, 183–256 (2017).
- 1253 47. Comstock, M. J., Ha, T. & Chemla, Y. R. Ultrahigh-resolution optical trap with single-  
1254 fluorophore sensitivity. *Nat. Methods* **8**, 335–340 (2011).
- 1255 48. Bustamante, C., Chemla, Y. R. & Moffitt, J. R. High-resolution dual-trap optical tweezers  
1256 with differential detection: an introduction. *Cold Spring Harb. Protoc.* **2009**, pdb.top60



- 1257 (2009).
- 1258 49. Berg-Sørensen, K. & Flyvbjerg, H. Power spectrum analysis for optical tweezers. *Rev. Sci.*  
1259 *Instrum.* **75**, 594–612 (2004).
- 1260 50. Wu, C., Read, C., McGeehan, J. & Crane-Robinson, C. The construction of customized  
1261 nucleosomal arrays. *Anal. Biochem.* **496**, 71–75 (2016).
- 1262 51. Kireeva, M. L., Lubkowska, L., Komissarova, N. & Kashlev, M. Assays and Affinity  
1263 Purification of Biotinylated and Nonbiotinylated Forms of Double-Tagged Core RNA  
1264 Polymerase II from *Saccharomyces cerevisiae*. *Methods Enzymol.* **370**, 138–155 (2003).
- 1265 52. Dangkulwanich, M. *et al.* Complete dissection of transcription elongation reveals slow  
1266 translocation of RNA polymerase II in a linear ratchet mechanism. *Elife* **2**, (2013).
- 1267 53. Bouchiat, C. *et al.* Estimating the Persistence Length of a Worm-Like Chain Molecule  
1268 from Force-Extension Measurements. *Biophys. J.* **76**, 409–413 (1999).
- 1269 54. Bustamante, C., Marko, J. F., Siggia, E. D. & Smith, S. Entropic elasticity of lambda-  
1270 phage DNA. *Science* **265**, 1599–600 (1994).
- 1271 55. Mills, J. B., Vacano, E. & Hagerman, P. J. Flexibility of single-stranded DNA: use of  
1272 gapped duplex helices to determine the persistence lengths of Poly(dT) and Poly(dA). *J.*  
1273 *Mol. Biol.* **285**, 245–257 (1999).
- 1274 56. Smith, S. B., Finzi, L., Bustamante, C. & Smith, S. Direct mechanical measurements of  
1275 the elasticity of single DNA molecules by using magnetic beads. *Science* **258**, 1122–6  
1276 (1992).
- 1277 57. Smith, S. B., Cui, Y. & Bustamante, C. Overstretching B-DNA: the elastic response of  
1278 individual double-stranded and single-stranded DNA molecules. *Science* **271**, 795–9  
1279 (1996).
- 1280 58. Wang, M. D., Yin, H., Landick, R., Gelles, J. & Block, S. M. Stretching DNA with optical  
1281 tweezers. *Biophys. J.* **72**, 1335–46 (1997).
- 1282

## 1 MAIN FIGURE LEGENDS

2

### 3 **Figure 1. Dual-trap Optical Tweezers Single-molecule Unzipping Assay Unwinds Nucleosomal** 4 **DNA and Maps Histone-DNA Interactions**

5 (A) Geometry of the single-molecule unzipping assay. Dashed arrows denote directions of trap  
6 movement (20 nm/s) during unzipping (red arrow) or reziping (black arrow). Two DNA handles  
7 connect to the template DNA, which consists of two tandem NPS repeats and an end hairpin. Diagram  
8 illustrates nucleosome unzipping, with the second NPS replaced with a pre-assembled  
9 mononucleosome. For simplicity, linkers and restriction sites flanking the NPS are not shown.

10 (B, C) Unzipping (red) and reziping (black) traces of bare NPS DNA (B) and a single WT human  
11 nucleosome (C). The presence of the nucleosome on the second NPS causes characteristic high force  
12 (20-40 pN) transitions that correspond to disruption of histone-DNA contacts. The unzipped basepairs  
13 (bp) are normalized to the beginning of the second NPS. The nucleosome reziping trace matches that  
14 of bare NPS DNA, indicating complete histone removal during unzipping.

15 (D) Representative unzipping traces of tetrasome (cyan), WT (red), H2A.Z (blue), and uH2B (green)  
16 nucleosomes. For clarity, only the region after entering the second NPS (corresponding to the boxed  
17 region in (C)) is shown, with the unzipped bp normalized to the beginning of the second NPS. The  
18 three dashed lines are entry, dyad, and exit of the second NPS, respectively. Reziping traces,  
19 identical to those of B and C, are not shown.

20 (E) Topography maps are plotted as force-weighted residence time (RT) histograms of the unzipping  
21 fork along bare NPS DNA, tetrasome and different types of nucleosomes during unzipping at constant  
22 trap separation speed of 20 nm/s. The grey histograms with colored stripes (excluding Bare NPS DNA  
23 and WT Nucleosome) are residual plots found by subtracting the WT nucleosome RTs. Unzipped bp  
24 are normalized to the beginning of the second NPS core. Major peaks are highlighted with grey  
25 dashed lines, with the peak positions (in bp) labeled above the peaks. (Left to right: 17, 22, 26, 31, 35,  
26 41, 52, 61, 69, 109, 112, 122 bp). n = 34, 41, 34, 39, 35, 10, respectively for NPS DNA, hWT, H2A.Z,  
27 M3\_M7, uH2B nucleosome and tetrasome.

28 See also Figure S1 for representative unzipping traces and analysis.

29

### 30 **Figure 2. Topography Maps of the Nucleosome Revealed by Nucleosome Unzipping at Constant** 31 **Force**

32 (A) Representative unzipping traces of bare NPS DNA (black), WT (red), H2A.Z (blue) and uH2B  
33 (green) nucleosomes at 28 pN constant force. Unzipped bp are normalized to the beginning of the  
34 second NPS. Dashed lines mark entry, dyad and exit regions of the second NPS. Traces are shifted  
35 horizontally for clarity.

36 (B) Mean residence time (RT) histogram of the unzipping fork along bare NPS DNA (black), WT  
37 (red), H2A.Z (blue) and uH2B (green) nucleosomes during unzipping at a constant force of 28 pN.  
38 Bare NPS RTs are too short to see on the axes shown. Unzipped bp are normalized to the beginning of  
39 the second NPS core. Major peak positions are indicated above each peak (in bp).  $n = 33, 17, 20, 20,$   
40 respectively for NPS DNA, WT, H2A.Z and uH2B nucleosomes.  
41 See also Figure S2 on assembly cooperativity of H2A.Z nucleosomes.

42

### 43 **Figure 3. Observation of Multiple Nucleosomal States at the Proximal Dimer Region**

44 (A) Time traces of number of base pairs unzipped (relative to beginning of the second NPS) with  
45 hWT nucleosome for fixed trap separations of 1031nm, 1045nm, and 1060nm (top to bottom).  
46 Color indicates increasing trap separation (purple to red), corresponding to clusters in Figure S3F.  
47 Grey dashed lines indicate 17, 23, and 28 base pairs unzipped.

48 (B) Probability distributions for the number of DNA bps unzipped, computed from force-extension  
49 data in Figure S3F. Each curve is from a different trap separation, matching colors in A and Figure  
50 S3F. Distributions are shown for both bare DNA (top) and WT nucleosome (bottom). Vertical black  
51 dotted line indicates the start of the second NPS. Vertical grey dashed lines indicate peak positions for  
52 bare DNA (with position in bp labeled), showing that WT nucleosome shifts the first peak within the  
53 NPS, and gives rise to an additional peak at 28 bp. See Figure S3F for force-extension data.

54 (C) Zoomed-in view of the black dashed box in (B). Peak positions are labeled in bp.

55 (D) DNA unzipping energy computed by assuming the unzipped bp distributions from data in Figure  
56 S3F (including distributions in B) correspond to equilibrium Boltzmann statistics. Inset  $\Delta E$  shows the  
57 DNA-octamer interaction energy, computed as the difference between unzipping energies in the  
58 presence of WT (red), H2A.Z (blue), and uH2B (green) nucleosomes and unzipping energies for bare  
59 DNA only (black). Vertical black dashed lines and \* indicate peak positions (labeled in bp).

60 See also Figure S3 on hopping traces and analysis of energy landscape from equilibrium data.

61

### 62 **Figure 4. A ‘Molecular Ruler’ Gauges the Positions of an Elongating Pol II with Near-Basepair** 63 **Accuracy**

64 (A) Experimental design of an improved single-molecule nucleosomal transcription assay. A single  
65 biotinylated Pol II (purple molecular structure) is tethered between two optical traps. Pol II  
66 transcription is measured as increases in distance between the two beads at 10 pN constant force. The  
67 inset box shows the composition of the template, which is constructed by ligating Pol II stalled  
68 complex (cyan), the molecular ruler (green), NPS DNA (or nucleosome, yellow-grey), and a short  
69 inter-strand crosslinked DNA (for stalling Pol II, red). The ‘molecular ruler’ consists of eight tandem  
70 repeats of a 64-bp DNA (green), each harboring a single sequence-encoded pause site.

71 (B) A representative trace of a single Pol II transcribing through a *Xenopus* WT nucleosome. The  
72 three black dashed lines indicate NPS entry, dyad and NPS exit, respectively. The inset shows a  
73 zoomed-in view of the boxed region, highlighting the repeating pause patterns within the ‘molecular  
74 ruler’. The grey dashed lines are the predicted pause sites, whereas the short green lines mark the  
75 actual pauses of Pol II.

76 (C) Zoomed-in view of Pol II dynamics within the NPS region of (B). The three black dashed lines  
77 indicate NPS entry, dyad and NPS exit, respectively. The right y-axis (in bp) is normalized to the  
78 beginning of the NPS. The left y-axis shows regions preceding the dyad as SHL in red. Black arrows  
79 indicates representative events of backtracking, pausing, productive elongation, and hopping. Regions  
80 corresponding to Pol II located at SHL(-5) and SHL(-1) are indicated with green and cyan dashed  
81 lines, with the corresponding Pol II-nucleosome complex structures plotted on top (PDB 6A5P for  
82 PolII-SHL(-5), 6A5T for PolII-SHL(-1)). Pol II, histones, template DNA, non-template DNA are  
83 colored in grey, green, red and blue, respectively.

84 See also Figure S4 on detailed characterization of the ‘molecular ruler’.

85

86 **Figure 5. High-resolution Trajectories of Individual Pol II Enzymes Transcribing through WT,**  
87 **H2A.Z and uH2B Nucleosomes**

88 (A, B) Representative traces of single Pol II enzymes transcribing through single human WT  
89 nucleosomes. The grey dotted lines are the pause sites within the ‘molecular ruler’. The inset (black)  
90 is the residence time of Pol II within the ‘molecular ruler’, highlighting repeating pausing signatures  
91 of Pol II. The three black dashed lines indicate NPS entry, dyad and NPS exit. Relative positions of  
92 Pol II on the template DNA are shown as a cartoon on the right. The traces in blue, green, red and  
93 cyan are examples of successful nucleosome crossing, while the trace in grey is an example of Pol II  
94 arrest in the nucleosome. For comparison, a trace of Pol II transcribing through bare NPS DNA  
95 (black) is shown on the left. Zoomed in traces of high-resolution Pol II dynamics within the NPS  
96 are shown in (B), highlighting (black arrowheads) long-lived pausing, backtracking and hopping events.  
97 The traces are shifted horizontally for clarity. The right y-axis is normalized to the beginning of the  
98 NPS, with the major pause positions marked (in bp) on the right.

99 (C, D) Representative traces of single Pol II enzymes transcribing through single human H2A.Z  
100 nucleosomes. (C) shows the full traces and (D) is a zoomed-in view of the high-resolution dynamics  
101 within the NPS region.

102 (E, F) Representative traces of single Pol II enzymes transcribing through single human uH2B  
103 nucleosomes. (E) shows the full traces and (F) is a zoomed-in view of the high-resolution dynamics  
104 within the NPS region.

105 See also Figure S5 on backtracking and hopping dynamics.

106

107 **Figure 6. Transcriptional Maps of the Nucleosome Reveal that H2A.Z Enhances the Width and**  
108 **uH2B the Height of the Barrier**

109 (A) Median residence time histograms of Pol II transcription through bare NPS DNA (black), xWT  
110 (orange), hWT (red), H2A.Z (blue) and uH2B (green) nucleosomes. Bar width is 1 bp and major peak  
111 positions are labeled (in bp) above the corresponding peaks. NPS entry, dyad, NPS exit are marked  
112 with blue dashed lines. The polar plots on the right are the corresponding transcriptional maps of the  
113 nucleosome, formed by projecting the residence time histogram onto the surface of nucleosomal DNA.  
114 The top axis (red) indicates corresponding positions of the first half of nucleosome expressed as  
115 superhelical locations (SHL).  $n = 35, 23, 26, 21, 31$ , respectively for NPS DNA, xWT, hWT, H2A.Z  
116 and uH2B nucleosomes.

117 (B) Crossing time (total time Pol II takes to cross the entire nucleosome region) distributions plotted  
118 using the complementary cumulative distribution function (CCDF, fraction of events longer than a  
119 given crossing time). Crossing times of Bare NPS DNA, Xenopus WT (xWT), human WT (hWT),  
120 uH2B and H2A.Z nucleosomes are plotted in black, orange, red, green and blue, respectively.

121 See also Figure S6 on statistics of the crossing time, crossing probability, pause-free velocity and  
122 arrest position.

123

124 **Figure 7. Mechanical Model for Pol II Transcription Through the Nucleosome**

125 (A) Schematic of the mechanical model, showing three different lengths of unwrapped DNA for a  
126 given polymerase position along the DNA sequence. The steric spheres are shown in purple  
127 (polymerase) and beige (nucleosome), while the DNA is shown as a tube. (i) shows a configuration  
128 with a short, sharply bent DNA linker connecting Pol II and the nucleosome, which are in contact and  
129 sterically pushing on each other. (ii) shows a medium-length straighter linker, with Pol II still pushing  
130 on the nucleosome. (iii) shows a long straight linker without contact between Pol II and the  
131 nucleosome. Linker DNA color corresponds to overall energy for each configuration (given in C).  
132 Black arrows represent tangent orientations of the DNA backbone at the point of polymerase binding  
133 (top) and for the last contact with the nucleosome (bottom). Linker length and bending angle (between  
134 indicated tangents) are labeled on each polymerase-nucleosome pair.

135 (B) Model of Pol II dynamics. Pairs (p,q) indicate the Pol II state: p indicates the length of the RNA  
136 transcript, and q the number of base pairs backtracked from the most recent main pathway state. Pol II  
137 steps forward one base pair with rate  $k_0$  or can enter a backtracked pathway by stepping backward one  
138 base pair at rate  $k_{b1}$ . From backtracked positions, Pol II can move forward a base pair with rate  $k_{fn}$  or  
139 can backtrack another base pair at rate  $k_{bn}$ . Moving forward from the first backtracked state returns Pol  
140 II to the main pathway.

141 (C) Energy landscape of nucleosome-Pol II interaction, for constant DNA-nucleosome interaction  
142 energies of  $1k_B T$  per base pair. DNA unwrapping decreases the DNA linker conformational energy,

143 while removing favorable DNA-nucleosome interactions, overall providing a minimum energy a few  
144 base pairs ahead of the front edge of Pol II. Forward Pol II steps are unfavorable as they shorten the  
145 DNA linker. Points *i*, *ii*, and *iii* correspond to configurations illustrated in A. Inset shows cross-section  
146 of energy landscape at Pol II position of 47 bp, highlighting the minimum in the energy landscape a  
147 few bps ahead of Pol II, at ~52 bps unwrapped. Pol II progress through the nucleosome is defined as  
148 the position of the Pol II center plus an additional 17 bp for consistency with the transcribed distance  
149 in Figure 6.

150 (D) Dwell time profiles for human WT, H2A.Z, and uH2B nucleosomes. Solid black lines are  
151 experimental mean dwell times and colored dotted lines are the best fitted mean dwell times according  
152 to the mechanical model.

153 (E) Estimated DNA-octamer interaction energy profiles for human WT, H2A.Z, and uH2B  
154 nucleosomes. The energy values are found such that they give the best fitted dwell times shown in (D).  
155 Peak positions referenced in the text are labeled in bp, relative to the start of the NPS.

156 See also Figure S7 for fitting of nucleosome energy profiles based on Pol II dwell times.

157

158 **SUPPLEMENTARY FIGURE LEGENDS**

159

160 **Figure S1. Unzipping Traces of Single Human WT, H2A.Z, M3\_M7, uH2B Nucleosomes and**  
161 **Tetrasomes.**

162 (A-E) Representative unzipping traces of WT nucleosomes (A), tetrasomes (B), H2A.Z nucleosomes  
163 (C), M3\_M7 nucleosomes (D) and uH2B nucleosomes (E). Reziping traces are not shown and they  
164 match bare NPS DNA reziping traces. The unzipped bp (basepairs) are normalized to the beginning  
165 of the second NPS core.

166 (F) Number of transitions per trace at the second NPS region. H2A.Z nucleosomes have on average  
167 one more transition per trace than WT or uH2B nucleosomes. A transition event is counted when the  
168 residence time peak is above an arbitrary threshold.

169 (G-H) Partial unzipping of H2A.Z (G) and WT (H) nucleosomes reveals no lateral mobility induced  
170 by multiple rounds of unzipping-rezipping. The unzipping fork repeatedly propagates to the proximal  
171 dimer region followed by reziping (not shown for clarity). The inset shows zoomed-in view of the  
172 boxed region, where the position of initial force rise remains unchanged. The dwelling of the  
173 unzipping fork in alternative positions (labeled above the dashed lines in bp) is consistent with  
174 hopping observed in this region.

175 (I) Native PAGE gels showing homogenous WT, H2A.Z and uH2B nucleosome samples used for  
176 single-molecule unzipping experiments.

177

178 **Figure S2. H2A.Z Nucleosomes Assemble More Cooperatively than WT nucleosomes**

179 (A) Sequence swaps between H2A and H2A.Z reveal important regions for hexasome formation. The  
180 native PAGE gel shows the propensity to form hexasomes during assembly of H2A, H2A.Z and  
181 swapped mutant nucleosomes. DNA is Cy5-labeled 70N0 where “N” denotes the 601 NPS. We found  
182 that this DNA configuration is more prone to hexasome formation due to the asymmetric nature of the  
183 601 sequence. Two octamer-to-DNA ratios are tested for each sample and are shown below its  
184 corresponding lanes. The nucleosome, hexasome or DNA bands are indicated on the right.

185 (B) Sequence alignment of H2A and H2A.Z swap mutants. Nomenclature of the swap mutants follows  
186 Clarkson *et al.*

187

188 **Figure S3. Hopping of the Unzipping Fork Near the Proximal Dimer Region of the Nucleosome**

189 (A, B) Unzipping traces of human WT nucleosome (A) and bare NPS DNA (B). Hopping near the  
190 proximal dimer region of WT nucleosome is indicated with a dashed blue square box; no similar  
191 hopping was observed in the corresponding region during unzipping of bare NPS DNA. Insets are the

192 zoomed-in view of the dashed square boxes. Unzipped bp is normalized to the beginning of the second  
193 NPS. Reziping traces are not shown for clarity.  
194 (C) Aligned individual force-extension curves (thin colored curves) and mean force-extension curve  
195 (thick black curve), for bare DNA.  
196 (D) Energy of DNA unzipping for each base pair, calculated from mean force-extension curve.  
197 (E) Comparison of experimental mean force-extension curve (blue) to the force-extension calculated  
198 from the extracted DNA unzipping energy (red).  
199 (F) Force-extension traces obtained at fixed trap separations with WT nucleosome. Color indicates  
200 increasing trap separation (purple to red), with number indicating the trap separation in nm.  
201 (G) DNA unzipping energy for each base pair, calculated from equilibrium hopping data at multiple  
202 fixed trap separations as in (F).  
203 (H) Comparison of experimental mean force-extension curve for bare DNA (black) and DNA with a  
204 WT nucleosome (red) to the force-extension curve predicted by the apparent DNA unzipping energy  
205 from equilibrium hopping data for the WT nucleosome (cyan).

206

#### 207 **Figure S4. Biochemical and Single-molecule Characterization of the “Molecular Ruler”**

208 (A) *In vitro* transcription assay identifies a major pause site within a single repeat sequence (64 bp).  
209 The band corresponding to the pause site is highlighted with a dotted red box. The sequence of the  
210 single repeat template DNA is shown above the gel, with the identified pause site highlighted in red.  
211 (B) Histogram of the length of one repeat unit (periodicity,  $d$ ). From aligned traces of Pol II  
212 transcription through xWT nucleosomes,  $d$  is calculated to be  $21.1 \pm 0.3$  nm.  
213 (C) Mean (black) and median (red) residence time (in log scale) of Pol II transcribing through the  
214 repeat sequence confirms a single major pause site at 59 bp in the repeat sequence, matching the site  
215 identified in (A).  
216 (D) Zoomed in view of the alignment of traces using the “molecular ruler” (cartoon on the right). The  
217 major pause site within each repeat sequence is marked with a grey horizontal line and a red dot next  
218 to the “molecular ruler”. Short horizontal black lines indicate identified pauses and vertical black lines  
219 (with the exception of few cases where the tether breaks in the middle) indicate the entry and exit of  
220 the “molecular ruler”.

221

#### 222 **Figure S5. Long-lived Pauses of Pol II in the Nucleosome are Associated with Backtracking and** 223 **Hopping Dynamics**

224 (A, B) Representative traces of backtracking (A) and hopping (B) dynamics of Pol II during  
225 transcription through an hWT nucleosome. The trace is the same as the red trace in Figure 5A, 5B.  
226 The black arrowheads in (A) highlight backtracking events right before long-lived pauses. The triple-  
227 stars highlight the region where Pol II has hopping dynamics, the zoomed in view of which is shown



228 in (B). The hopping trace is fitted as two states with a classic hidden Markov model (red is raw data,  
229 black is fitted trace). The fitted parameters and histogram of Pol II position counts are shown to the  
230 right side.  $d$  is the distance transcribed,  $p$  is the probability in that state, and  $k_{\text{out}}$  is the rate of  
231 transitioning to the other state.

232 (C, D) Representative traces of backtracking (C) and hopping (D) dynamics of Pol II during  
233 transcription through an H2A.Z nucleosome. The trace is the same as the orange trace in Figure 5C,  
234 5D. The data is analyzed and shown as in (A, B)

235 (E, F) Representative traces of backtracking (E) and hopping (F) dynamics of Pol II during  
236 transcription through an uH2B nucleosome. The trace is the same as the grey trace in Figure 5E, 5F.  
237 The data is analyzed and shown as in (A, B) except that the trace in (F) is fitted as three-states.

238

239 **Figure S6. Crossing Time, Crossing Probability and Pause-free Velocity of Pol II during**  
240 **Transcription through NPS DNA or Nucleosomes**

241 (A-E) Histograms of crossing time of Pol II transcription through bare NPS DNA (A), xWT (B), hWT  
242 (C), H2A.Z (D) and uH2B (E) nucleosomes. See also Figure 6B.

243 (F) Relative percentage of Pol II molecules that are arrested or crossed during transcription through  
244 bare NPS DNA or nucleosomes.

245 (G) Pol II arrest positions within the NPS. The positions are normalized to the beginning of the NPS.  
246 Each dot is a single arresting event. The percentages of arresting before or after dyad are shown below  
247 the dots.

248 (H) Pause-free velocity of Pol II molecules before, inside and after NPS during transcription through  
249 bare NPS DNA, and xWT, hWT, H2A.Z and uH2B nucleosomes. Only traces that reached the stall  
250 site at the end of the template are considered. Pause-free velocities are calculated in three fastest  
251 regions (to partially correct for velocity differences due to sequence variations) up to 100 bp before,  
252 inside, and up to 100 bp after NPS.

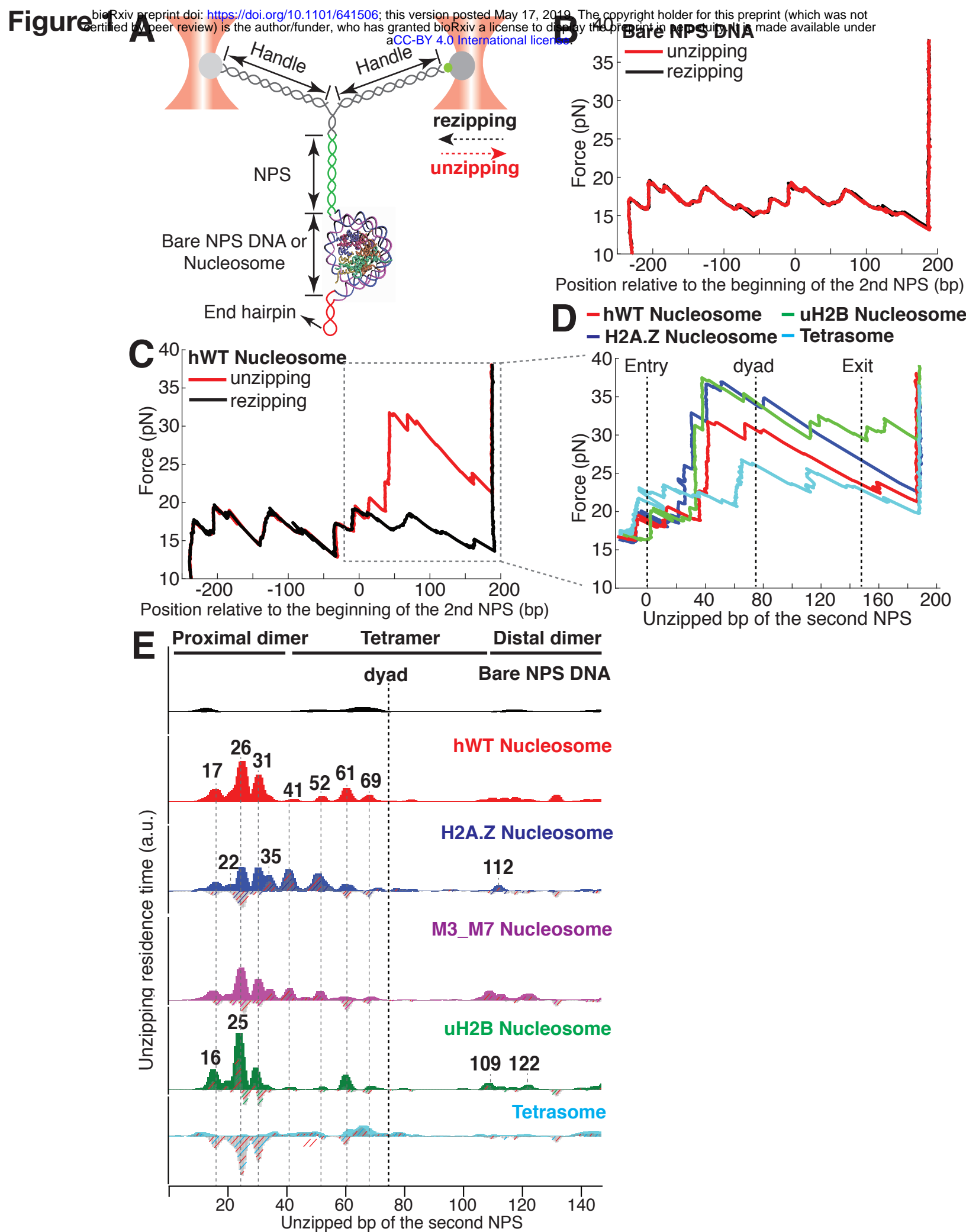
253

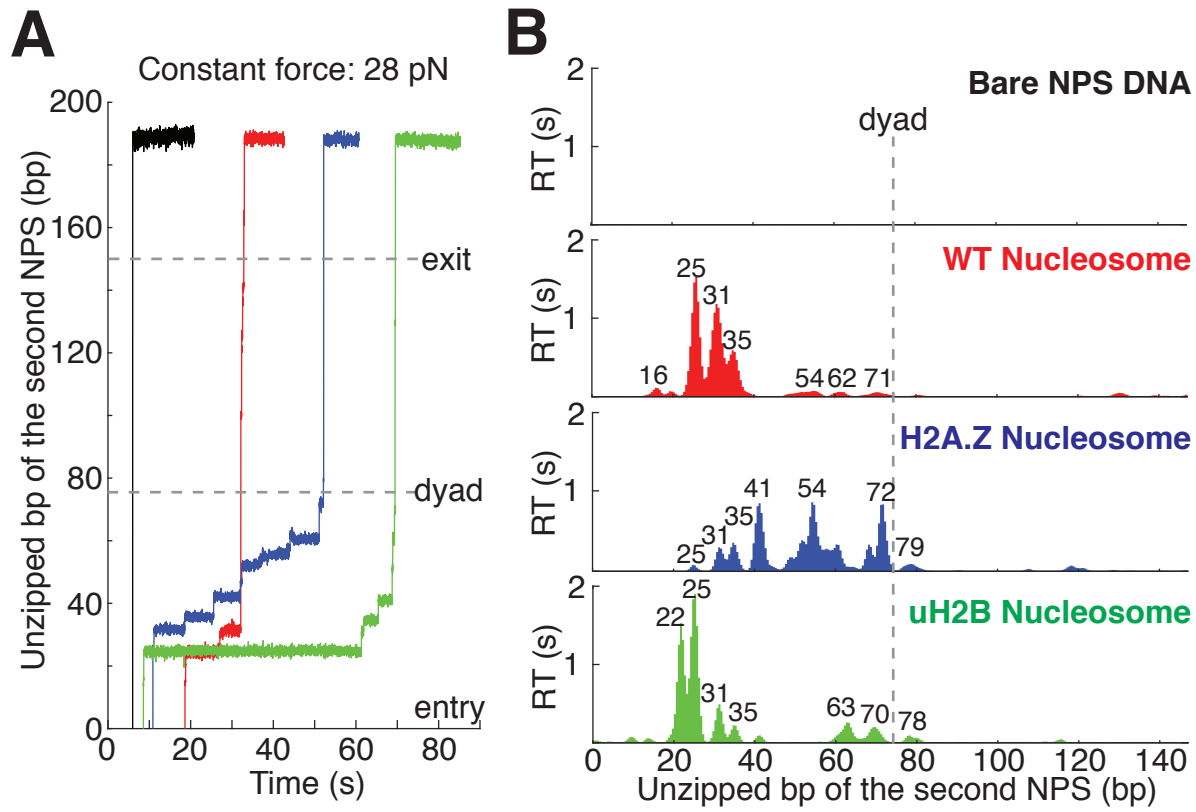
254 **Figure S7. Fitting Nucleosome Energy Profiles Based on Pol II Dwell Times**

255 (A-C) Mean dwell times (colored dotted lines) calculated from best-fit mechanical model (see Figure  
256 7 D-E) whose corresponding nucleosome binding energies (insets, colored lines) are shown for (A)  
257 hWT, (B) H2A.Z, and (C) uH2B nucleosomes. The black dashed lines of the inset are binding energy  
258 data obtained from unzipping under equilibrium conditions (hopping, see Fig 3D inset), and black  
259 dashed lines of the main plots are dwell times calculated from these energy landscapes. The hopping  
260 data covers a narrow region of sequence, and therefore allows prediction of Pol II pausing only at the  
261 start of the NPS.

262 (D) The experimental (black lines) and calculated mean dwell time (dotted line in magenta) for  
263 *Xenopus* WT (xWT) nucleosome, with the energy landscape extracted from the experimental mean

264 dwell time using the same procedure as for hWT, H2A.Z, and uH2B (Fig 7D). Inset compares hWT  
265 (red) and xWT (magenta) energy landscapes.  
266  
267





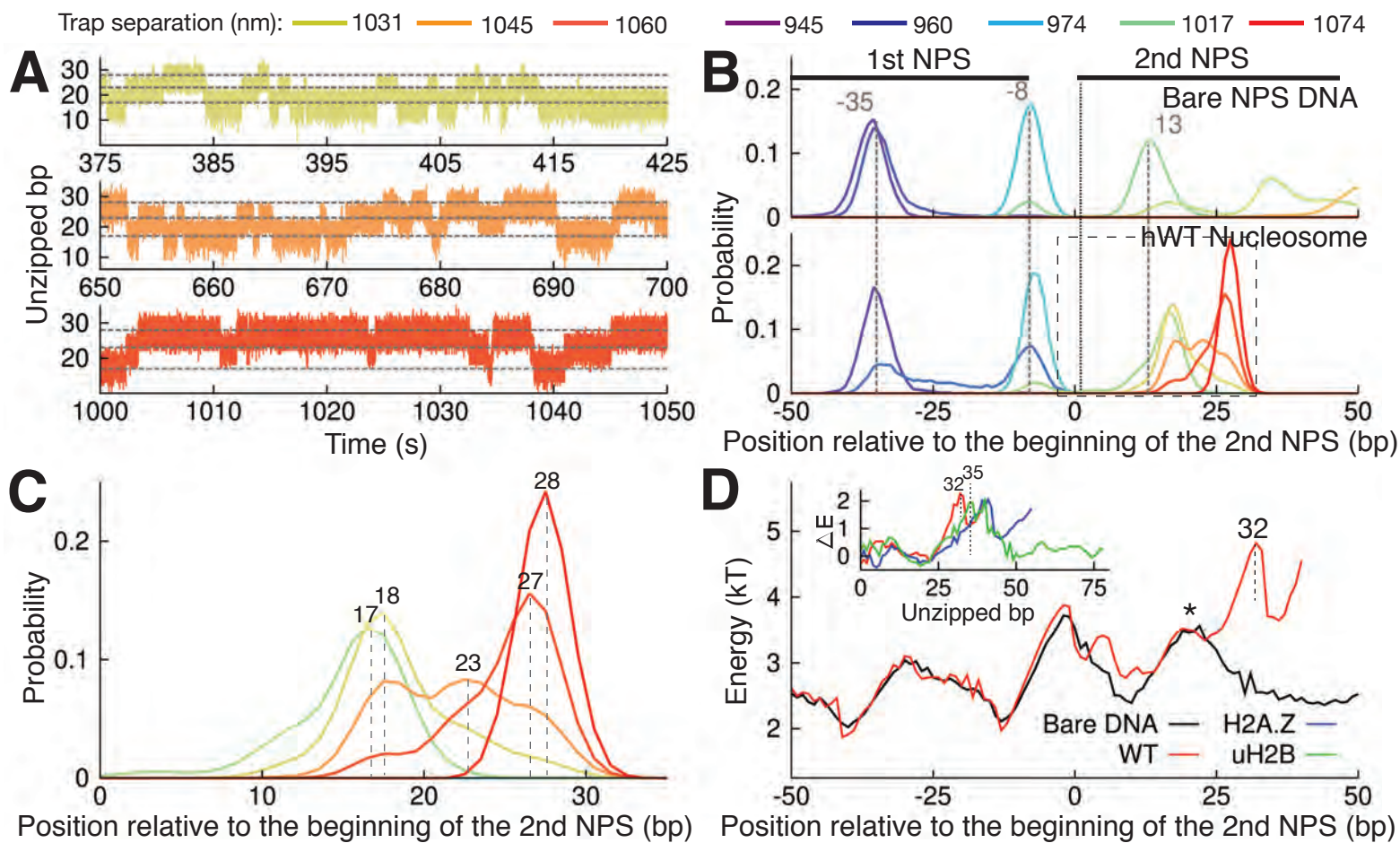


# Figure 4

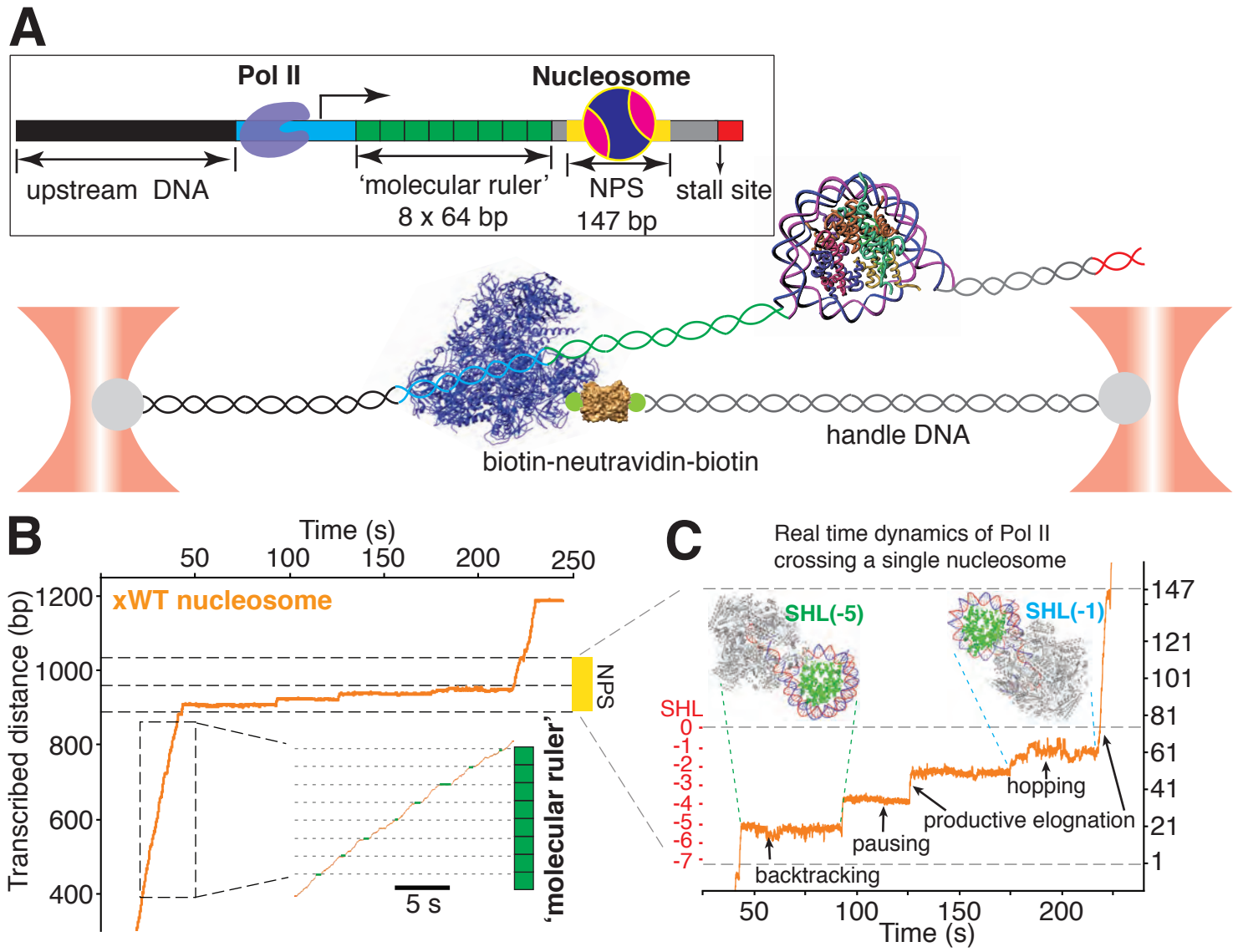


# Figure 6

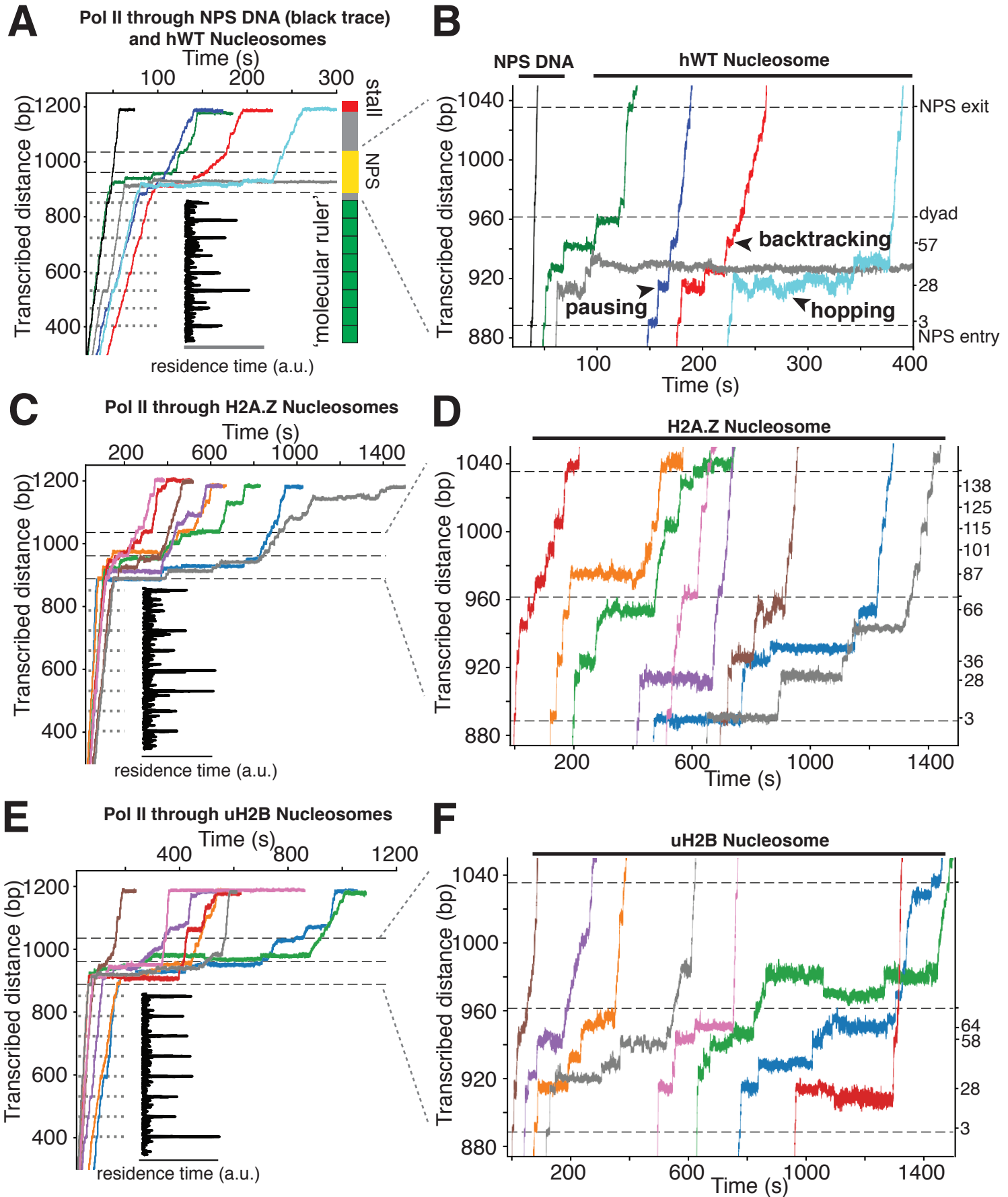


# Figure 6

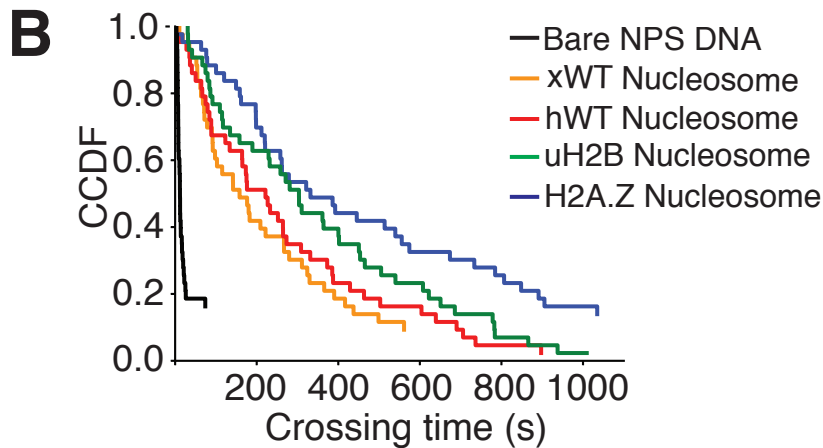
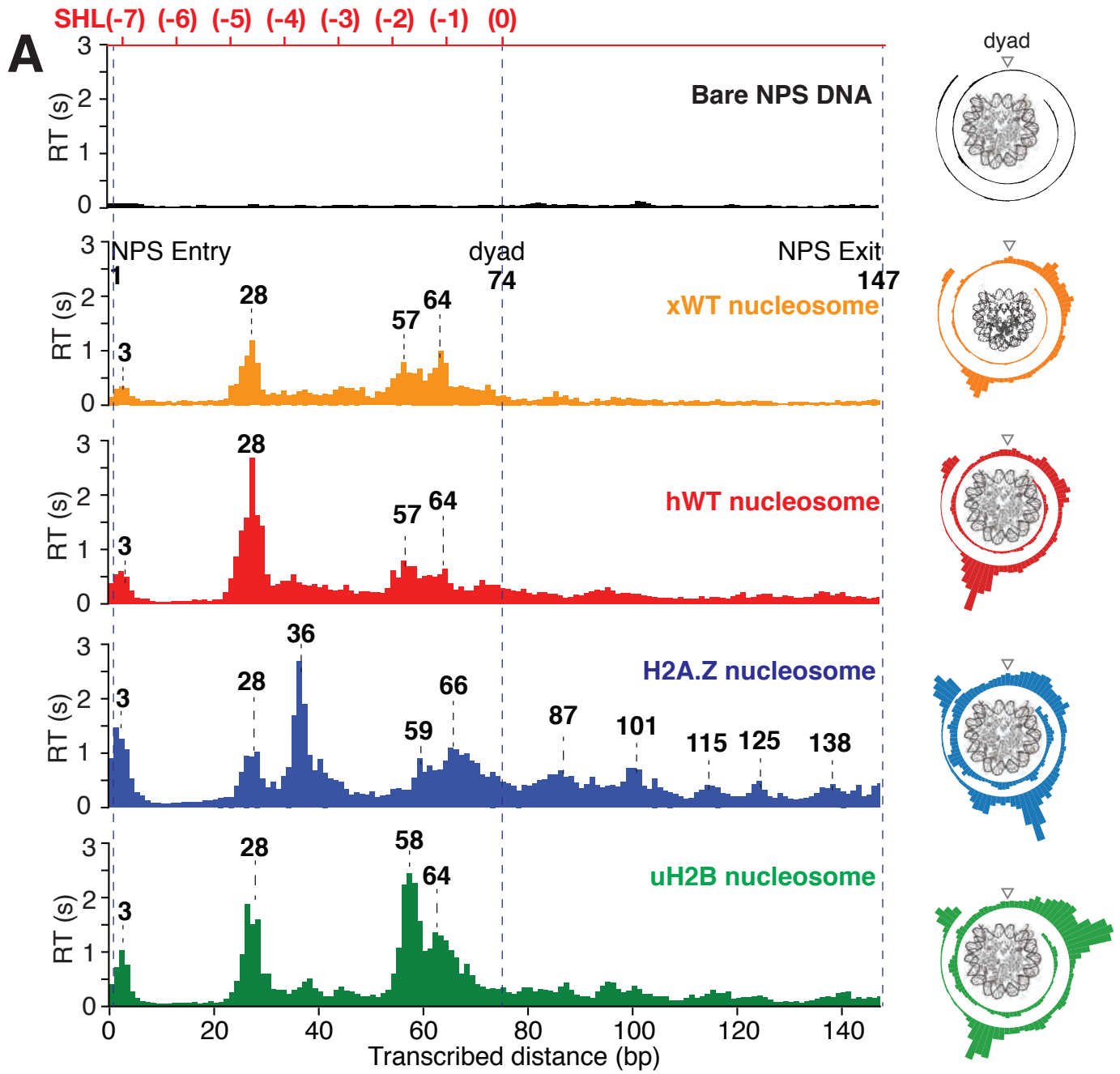




# Figure 7

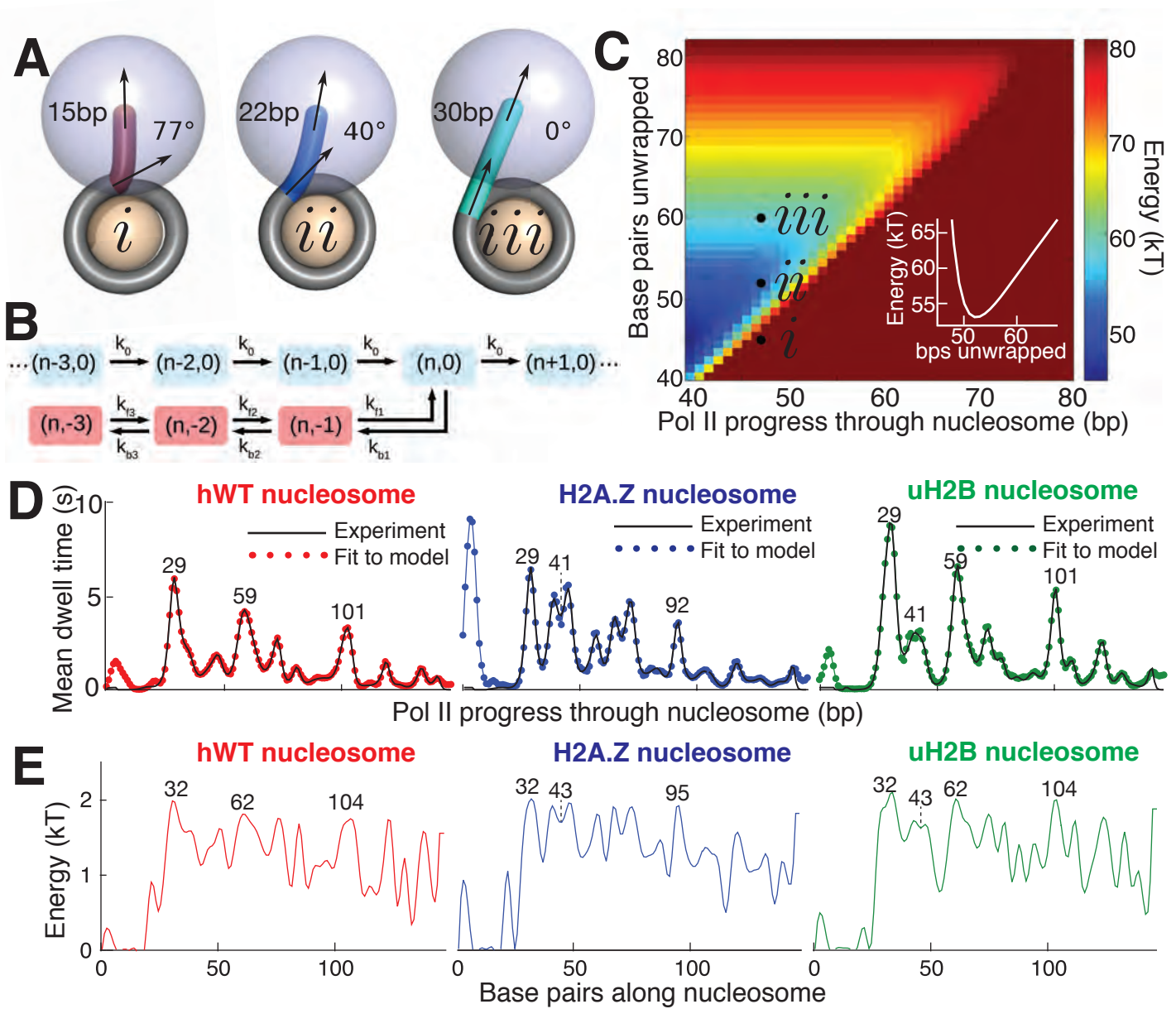
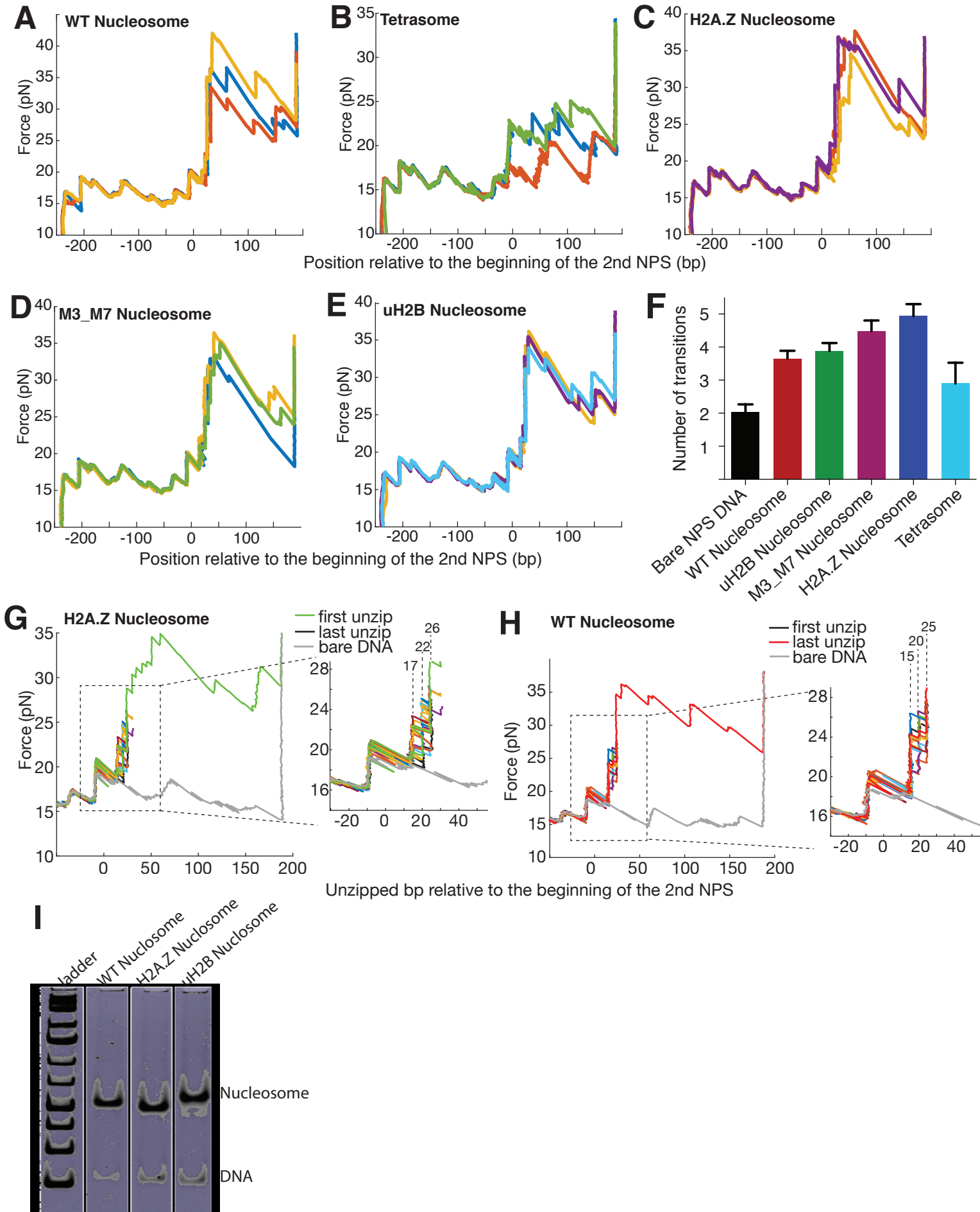
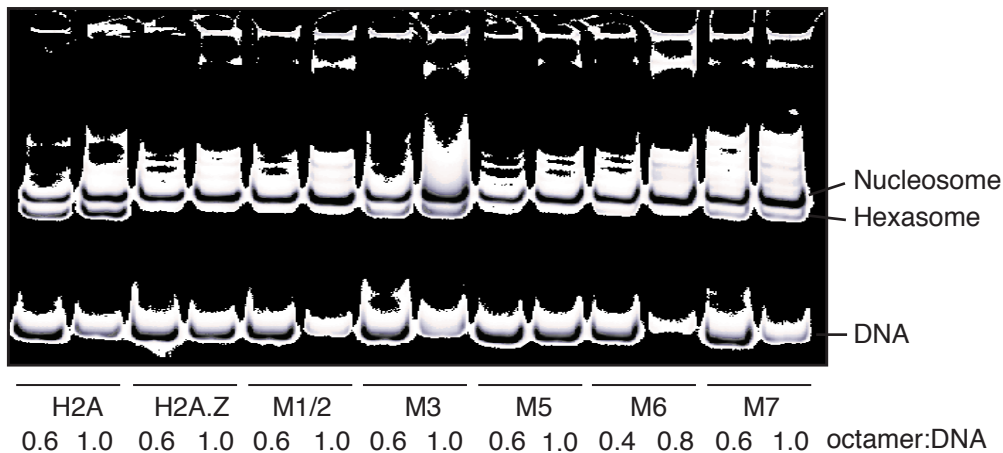


# Figure S1



**A**



**B**

H2A	MSG---RGKQGGKARAKAKSRSS----	RAGLQFPVGRVHRLLRK-GNYAERVGAGAPVYL	52
H2A.Z	MAG-GKAGKDSGKAKTKAVSRSQ----	RAGLQFPVGRIHRHLKSRTTSHGRVGATAAVYS	55
H2A.Z_M6	MAG-GKAGKDSGKAKTKAVSRSQ----	RAGLQFPVGRIHRHLKSRTTSHGRVGATAAVYS	55
H2A.Z_CT	MAG-GKAGKDSGKAKTKAVSRSQ----	RAGLQFPVGRIHRHLKSRTTSHGRVGATAAVYS	55
H2A.Z_M7	MAG-GKAGKDSGKAKTKAVSRSQ----	RAGLQFPVGRIHRHLKSRTTSHGRVGATAAVYS	55
H2A.Z_M1/2	MSG---RGKQGGKARAKAKSRSS----	RAGLQFPVGRVHRLLRK-GNYAERVGAGAPVYL	52
H2A.Z_M3	MAG-GKAGKDSGKAKTKAVSRSQ----	RAGLQFPVGRIHRHLKSRTTSHGRVGATAAVYS	55
H2A.Z_M5	MAG-GKAGKDSGKAKTKAVSRSQ----	RAGLQFPVGRIHRHLKSRTTSHGRVGATAAVYS	55
H2A	AAVLEYLTAEILELAGNAARDNKKTRIIIPRHLQLAIRNDEELNKLGRVTIAQGGVLPNI	112	
H2A.Z	AAILEYLTAEVLELAGNASKDLKVKRITPRHLQLAIRGDEELDSL-KATIAGGGVIPHI	114	
H2A.Z_M6	AAILEYLTAEVLELAGNASKDLKVKRITPRHLQLAIRGDEELNKLGRVTIAQGGVLPNI	112	
H2A.Z_CT	AAILEYLTAEVLELAGNASKDLKVKRITPRHLQLAIRGDEELDSL-KATIAGGGVIPHI	114	
H2A.Z_M7	AAILEYLTAEVLELAGNASKDLKVKRITPRHLQLAIRGDEELDSL-KATIAGGGVIPHI	114	
H2A.Z_M1/2	AAILEYLTAEVLELAGNASKDLKVKRITPRHLQLAIRGDEELDSL-KATIAGGGVIPHI	114	
H2A.Z_M3	AAILEYLTAEVLELAGNASKDLKVKRITPRHLQLAIRGDEELDSL-KATIAGGGVIPHI	114	
H2A.Z_M5	AAILEYLTAEVLELAGNAARDNKKTRITPRHLQLAIRGDEELDSL-KATIAGGGVIPHI	114	
H2A	QAVLLPKKTESHHKAKGK-----	130	
H2A.Z	HKSLIGKKGQKQTV-----	128	
H2A.Z_M6	HKSLIGKKGQKQTV-----	128	
H2A.Z_CT	QAVLLPKKTESHHKAKGK-----	130	
H2A.Z_M7	QAVLIGKKGQKQTV-----	128	
H2A.Z_M1/2	HKSLIGKKGQKQTV-----	128	
H2A.Z_M3	HKSLIGKKGQKQTV-----	128	
H2A.Z_M5	HKSLIGKKGQKQTV-----	128	

# Figure S3

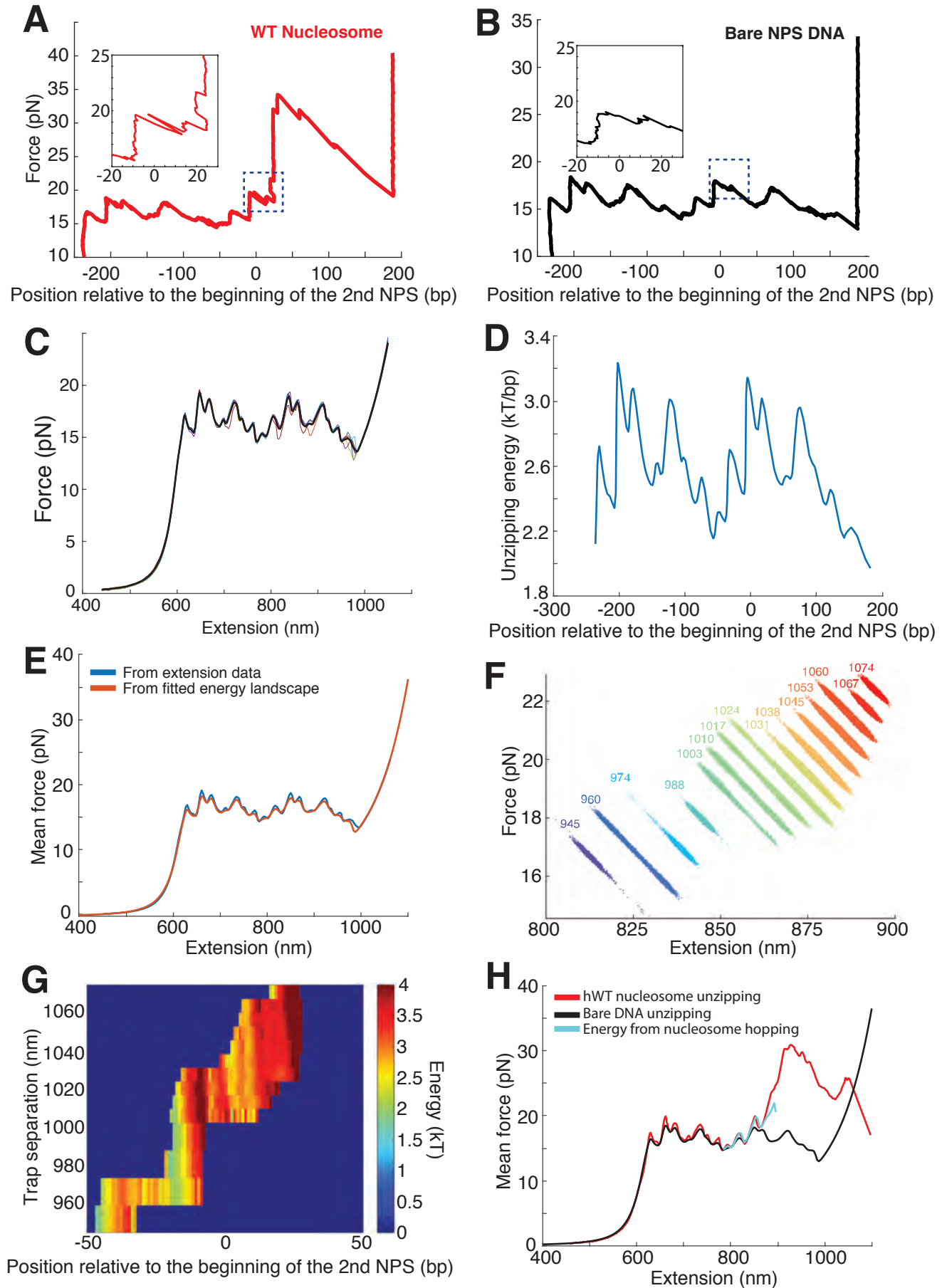


# Figure S4

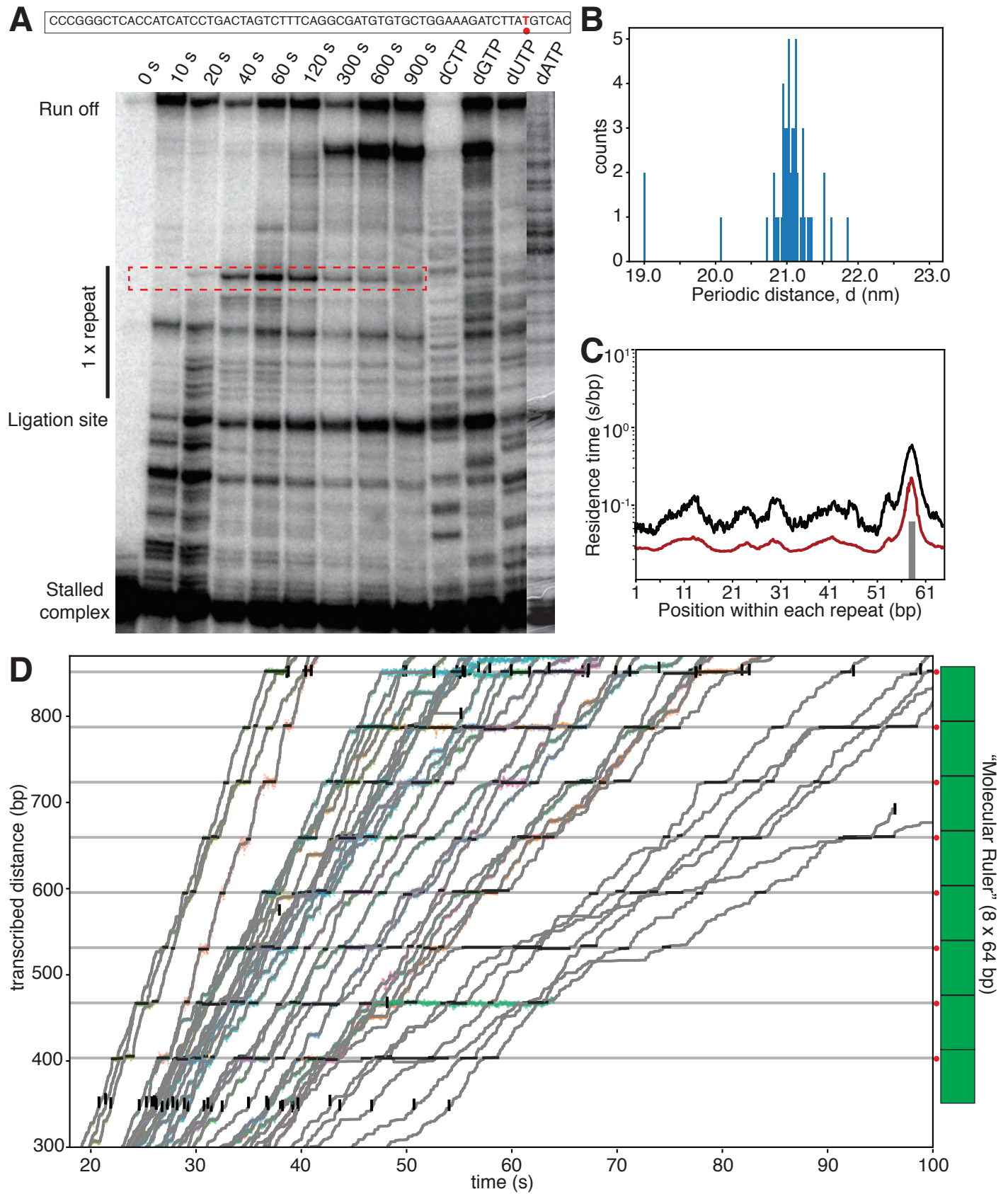


# Figure S5

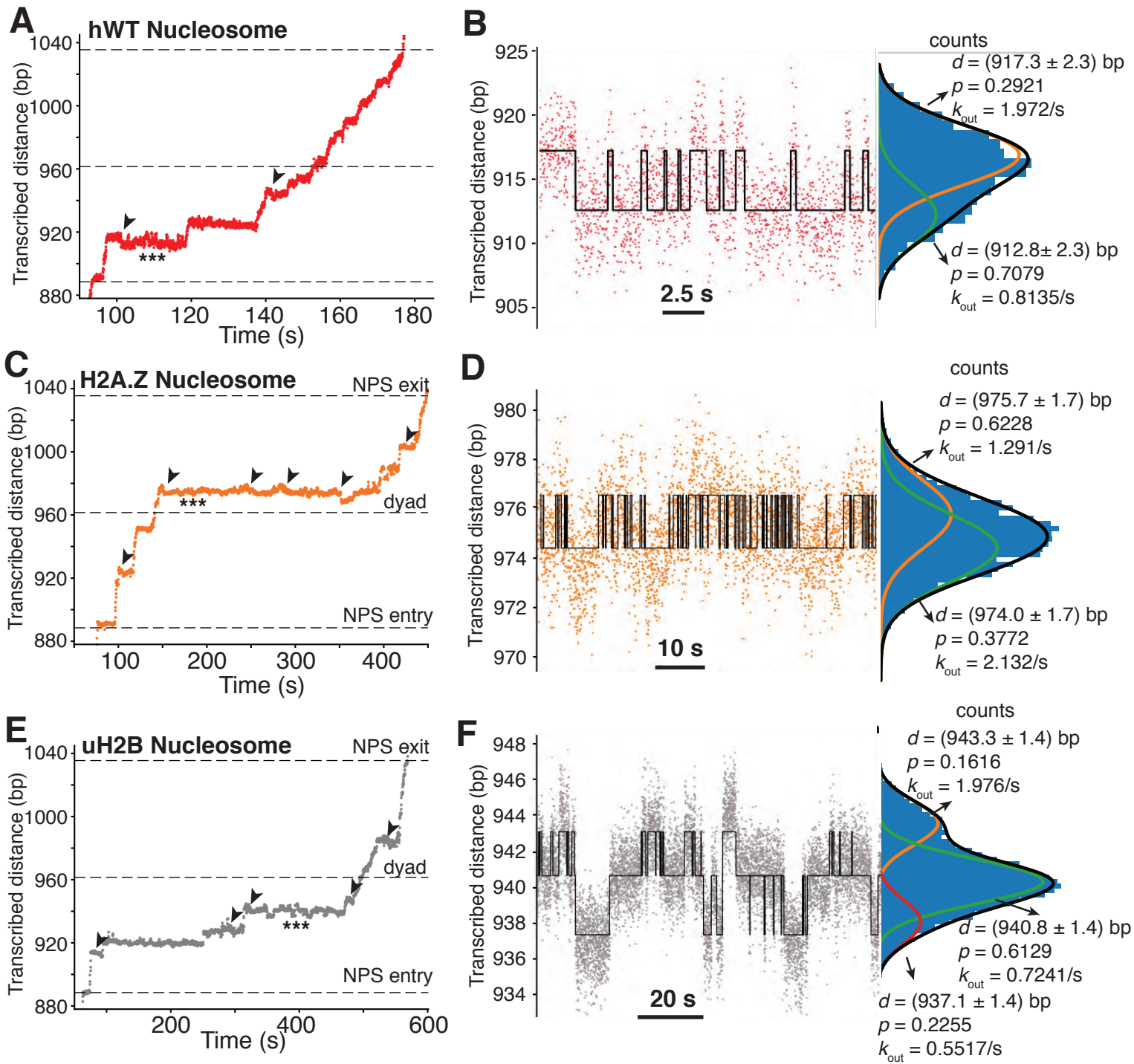


# Figure S6

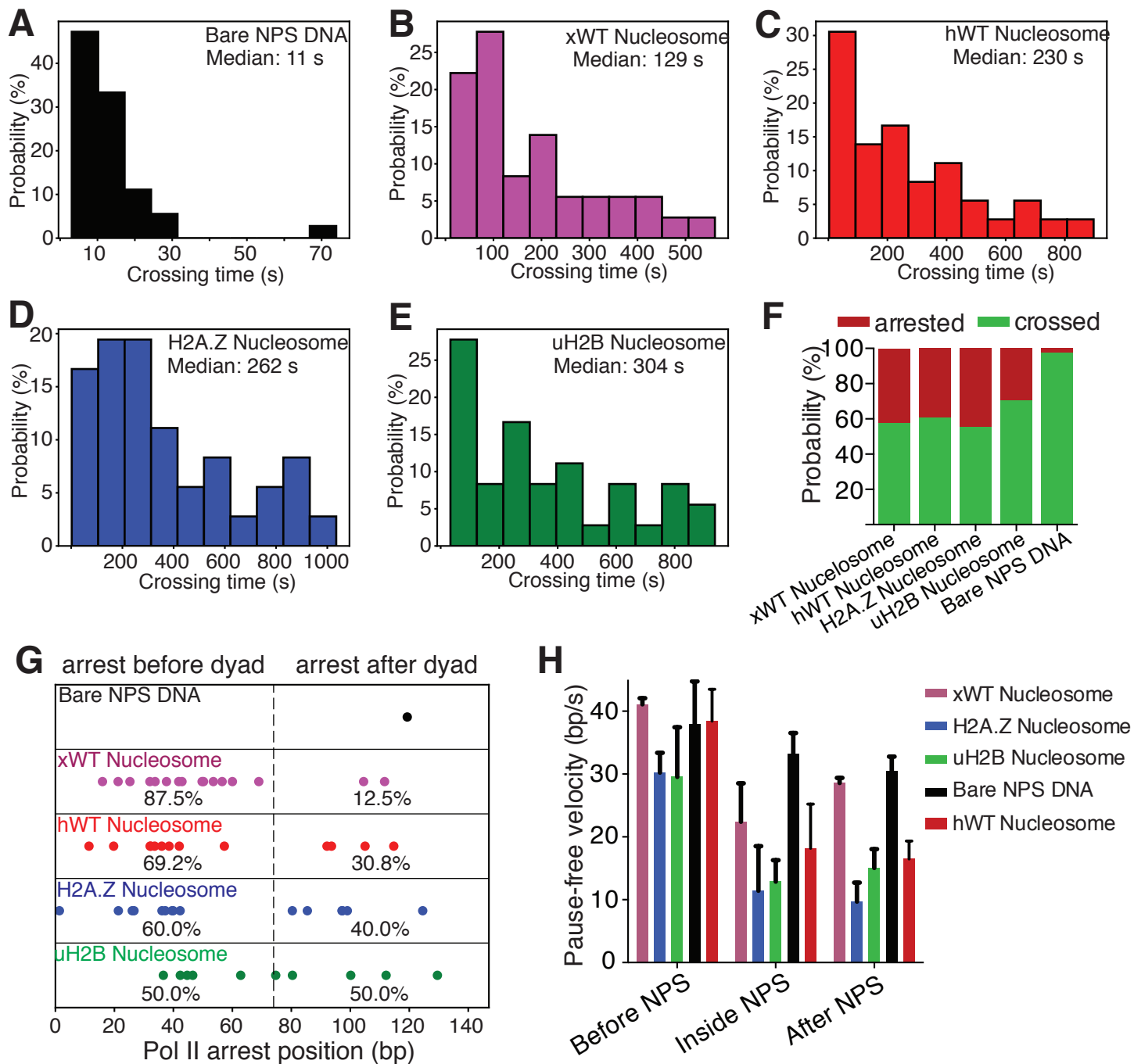


# Figure S7

